X-641-71-145
PREPRINT

IONIZATION OF MULTI ELECTRON ATOMS BY FAST CHARGED PARTICLES

K. OMIDVAR
H. L. KYLE
E. C. SULLIVAN

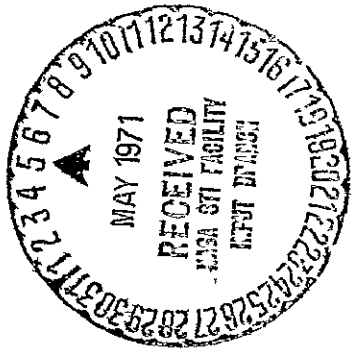

APRIL 1971

GODDARD SPACE FLIGHT CENTER
GREENBELT, MARYLAND

IONIZATION OF MULTI ELECTRON ATOMS BY FAST CHARGED PARTICLES

K. Omidvar, H. L. Kyle, and E. C. Sullivan
Laboratory for Space Physics
NASA-Goddard Space Flight Center
Greenbelt, Maryland 20771

Ionization of five inert gas atoms, five alkalides, atomic magnesium, zinc, carbon, nitrogen, and oxygen, and lithium ions by electron impact have been considered and the total atomic cross section due to single ionization from all shells have been calculated. Differential cross sections for ionizaiton of helium and neon by electron impact, differential cross section for ionization of helium by proton impact, and photoionization of lithium have been calculated. Comparison is made with the available experimental data. Calculation is based on the Born approximation and a central field approximation for the active atomic electron. The active electron is described before ejection by a Coulomb function with an effective charge given by the Hartree-Fock calculation, and is described by a Coulomb function with a charge of unity after ejection. Agreement found with a wide range of experimental data for the differential and the total cross sections is much better than might be suggested by the model of calculation, and in many cases better than the more sophisticated calculational models.

The yield for the production of doubly charged ions in collision of electrons with kryton, sodium, potassium, rubidium, cesium, and magnesium based on a suggested mechanism has been calculated, and in a number of cases satisfactory agreement is found with the experimental data.

I. INTRODUCTION

There have been numerous calculations on atomic ionization by charged particles. All these calculations are different approximations to a problem that cannot be formulated easily. An important case to mention is ionization of a hydrogen atom by an electron. Since the quantum mechanical wave function of a system of two free electrons and a proton in the asymptotic region of the configuration space for low impact energies is not known, for the ionization cross section no correct functional form or expression which can yield itself to numerical evaluation is available. At the threshold of ionization the problem has been solved classically by Wannier[1] with certain validity.

Here we consider the high impact energy ionization of multiple electron atoms by charged particles. Since in this problem the asymptotic form of the system's wave function is well known, an expression for the ionization amplitude can be found, and with increasing computational labor more and more accurate values for the cross section can be obtained.

A distinction between the ionization of a many electron atom from that of the hydrogen atom is the presence of multiple excitation and multiple ionization in the many electron case. When resonance scattering for single or multiple excitations occurs, giving rise to autoionization, there is an increase in the ionic current for certain impact energies, and several maxima are seen in the measured ionization cross sections. Another distinction is the interference phenomena of the waves that are scattered from different atomic electrons in

the case of the many electron atoms. For heavy atoms and molecules whose structure resembles a crystal this is an important phenomena. However, diffraction is more important for elastic scattering. Also, at high impact energies where the wave number of the relative motion is many times smaller than the atomic radius, diffraction is negligible, and independent particle model as is used in this calculation are justifiable.

Concerning ionization calculation of a many electron atom system, aside from the Born approximation, a class of such calculations is the so called binary encounter classical calculations. A review of the subject is given by Vriens[2]. In these calculations the target atom is described by a single state. Such a model is simpler than the Born approximation where the target atom is described by an initial and a final state. A serious defect of a single state model is its inability to produce the important dipole potential field acting on the scattered electron which is present in almost all inelastic collisions. This potential is due to the fact that quantum mechanically the target is described by a mixture of the initial and final states atomic wave functions. Due to this potential in accordance with experiment the inelastic cross section at high energy behaves as $A \ln(CE)/E$ where A and C are some atomic constants and E is the impact energy. Since this coupling does not exist in the classical theory, this theory is incapable of giving correct results at high impact energies.

A correct calculation within the Born approximation requires the knowledge of the initial and final atomic state wave functions. While the initial wave functions are available in the Hartree-Fock approximation, an accurate final state wave function, where the ejected electron is not bound to the atom, is not easily obtainable. As a result a complete Born calculation does not seem to be available.

McDowell[3] and Peach[4] have made an approximation to the Born approximation by describing the final state as the product of a Hartree-Fock wave function for the residual ion and a Coulomb wave function for the ejected electron. Implicit in this approximation is that the initial and final states of the atom have different Hamiltonians. More specifically, the active atomic electron is in a non Coulombic potential before ejection and in a Coulomb potential after ejection. They have applied this approximation to the impact ionization calculation of a large number of elements.

A more recent calculation within the Born approximation is due to McGuire[5] where the active electron is acted upon by a central Coulomb potential with variable charge. The model is used to calculate a number of atomic ionization cross sections.

In the model used here[6] we describe the active atomic electron before and after ejection by a Coulomb wave function. The initial state is then described by an hydrogenlike eigenfunction whose quantum numbers are specified by the

configuration of the atom and whose Coulomb charge is obtained from a Hartree-Fock calculation as will be described later. This charge from here on will be referred to as the effective charge Z_e. The final state is described by a Coulomb function with central charge unity. Since the effective charge is different from unity the two states of the active electron don't belong to the same Hamiltonian. Improvement in the model results if a posteriori the wave functions are made orthogonal to each other, as if the two states had the same Hamiltonian. This is done by the conventional method of adding some of the initial state wave function to that of the final state.

An approach similar to ours has been taken by Burhop[7] and a number of other authors. According to these authors the active electron is both initially and finally in a Coulomb field with the same effective charge; thus no orthogonalization of the states is necessary. We believe that this is not a good approximation in view of the fact that the long range dipole potential mentioned previously plays an important role at high impact energies, and in the model of Burhop and others the dipole moment in the potential is smaller than it should be. To see this we notice that the time spent by the atomic electron in traversing the diameter of the atom before ejection is much smaller than the time spent by the scattered electron in the dipole potential field. An appropriate final state for the atomic electron would then be a Coulomb function with central charge equal to unity. The effective charges used by Burhop and others are greater than unity. This would lead to a dipole moment for the long range potential

smaller than the dipole moment used in the present paper, and this leads to cross sectional values which at high energies will be smaller than those calculated here. Comparison with the experimental data to be discussed later shows that we have satisfactory agreements with measurements for a large number of cases at high impact energies.

We now summarize the results obtained here. Among the inert gases the ionization cross section by electron for helium, neon, argon, krypton, and xenon have been calculated. In alkalides similar calculation has been done for lithium, sodium, potassium, rubidium, and cesium. Total cross section for electron impact ionization of magnesium, zinc, carbon, oxygen, and nitrogen have also been calculated and given. In all cases the ionization cross section of not only the outermost shells but all the shells that have contributed appreciably to the cross section have been calculated. All calculated results have been compared with those of experiments and interpretations have been made accordingly.

A critical test for the validity of the model is comparisons between calculated and measured differential cross sections per unit energy range of the ejected electrons. Here this comparison is made for protons on helium, and electrons on helium and neon where the measurements have recently become available.

Similarly, it is instructive to compare calculated photoionization cross sections based on the present model with measurement. Since photoionization

cross section has the same functional form as the high impact energy cross section per unit energy range of the ejected electrons, this comparison will also give some information about the accuracy of the model. Here we have calculated photoionization of lithium, and have made a comparison with the experimental results.

It will also be interesting to see the degree of validity of the model for ionization of ions. For this reason we have calculated ionization of lithium ion by electron impact and have compared calculation with measurement.

Finally, we like to mention the limitations of the present model, and also of the Born approximation. Since the difference between the two Hamiltonians of the atomic states in the present model is proportional to the difference in the two Coulombic charges, when the initial effective charge is greatly different from unity, the approximation will not be a good one. Then the model provides a better approximation for the outer shell electron ionization than the inner shells. From the point of view of the relativistic theory, for some inner shells $Z_e/137$ is not small compared to unity, and the Dirac's theory should be used to obtain the atomic wave functions. On the other hand the central field approximation is invalid for description of the outer shell electron wave functions in the heavy elements. Some other approximations, like that of Thomas Fermi model, should be used to obtain these wave functions.

II. FORMULATION

The cross section per unit energy range of the ejected electrons, $d\sigma/d\epsilon$, in the Born approximation and according to the model discussed before in ionizing collision of a charged particle with charge Z'e, e being the electronic charge, with an atom with an active electron specified by the principal and the azimuthal quantum numbers n and ℓ is given by

$$\frac{d\sigma}{d(\epsilon/Ry)} = \frac{4\pi M Z'^2}{(2\ell+1) m_e a_0^3} \frac{\sqrt{\epsilon/Ry}}{E/Ry} \int_{K_1-K_2}^{K_1+K_2} \frac{dq}{q^3} \sum_{m=0}^{\ell} |\langle f | e^{i\vec{q}\cdot\vec{r}} | n\ell m \rangle|^2 d\hat{K} \quad (1)$$

with σ the total cross section in units of a_0^2, ϵ the energy of the ejected electron, E and M the relative energy and reduced mass of the colliding system, and m_e the electronic mass. k_1 is the wave number of the relative motion before collision related to E by

$$K_1^2 = a_0^{-2} (M/m_e)(E/Ry) \quad (2)$$

and k_2 is the wave number of the relative motion after collision related to k_1 by

$$K_1^2 - K_2^2 = a_0^{-2} (M/m_e)(\Delta E/Ry) \quad (3)$$

with ΔE the excitation energy. $\hbar\mathbf{q} = \hbar(\mathbf{k}_1 - \mathbf{k}_2)$ is the momentum transfer between the particles, m is the absolute value of the magnetic quantum number of the atomic electron, and $\hat{k}$ is a unit vector in the direction of the ejected electron. The final state vector $|f\rangle$ is given by

$$|f\rangle = |\vec{K}\rangle + Y|n\ell m\rangle \quad (4)$$

where $|k\rangle$ is a Coulomb wave function with charge unity normalized such that asymptotically it behaves as $(2\pi)^{-3/2}\ \exp(i\,k\cdot r)$ with r the position vector of the atomic electron. The constant γ is given by

$$\gamma = -\langle \vec{k} | n\ell m\rangle \tag{5}$$

so that $\langle f | n\ell m\rangle = 0$, as required. The momentum of the ejected electron is k and is related to ϵ by the relation

$$|\vec{k}|^2 = a_0^{-2}(\epsilon/Ry) \tag{6}$$

It is easy to see that σ has the correct dimension as required.

From (4) and (5) we have that

$$\langle f | e^{i\vec{q}\cdot\vec{r}} | n\ell m\rangle = \langle \vec{k} | e^{i\vec{q}\cdot\vec{r}} | n\ell m\rangle - \langle \vec{k} | n\ell m\rangle \langle n\ell m | e^{i\vec{q}\cdot\vec{r}} | n\ell m\rangle \tag{7}$$

It is easier to evaluate the first matrix on the right hand side of (7) in parabolic coordinates and then transform it to the spherical coordinates. If the state vectors in the parabolic coordinates be specified by $|nn_1m\rangle$, with n_1 the usual quantum number in parabolic coordinates, then it follows immediately that

$$\langle \vec{k} | e^{i\vec{q}\cdot\vec{r}} | n\ell m\rangle = \sum_{n_1=0}^{n-m-1} \langle \vec{k} | e^{i\vec{q}\cdot\vec{r}} | nn_1m\rangle \langle nn_1m | n\ell m\rangle \tag{8}$$

where the coefficients $\langle nn_1m | n\ell m\rangle$ are given through the Wigner's 3j symbol by [8,9]

$$\langle n n_1 m | n l m \rangle = (-)^m (2l+1)^{1/2} \begin{pmatrix} \frac{1}{2}(n-1) & \frac{1}{2}(n-1) & l \\ \frac{1}{2}(m-n_1+n_2) & \frac{1}{2}(m+n_1-n_2) & -m \end{pmatrix} \quad (9)$$

with n_2 the other quantum number in parabolic coordinates related to n_1 by the relation $n_1 + n_2 = n - m - 1$. The value of the matrix $\langle k | \exp(iq \cdot r) | n n_1 m \rangle$ is given below.

$$\langle \vec{k} | e^{i \vec{q} \cdot \vec{r}} | n n_1 m \rangle = \frac{(2i\alpha)^{m+2} e^{im\varphi_1}}{2\sqrt{\pi Z e}} \left[\frac{(n_2+m)!}{(n_1+m)! n_1! n_2!} \right]^{1/2}$$

$$\times \left(\frac{\beta}{1 - e x p(-2\pi\beta)} \right)^{1/2} q^m \left[1 - (\hat{q} \cdot \hat{k})^2 \right]^{\frac{m}{2}} A^{-m+i\beta} B^{-1-i\beta} \sum , \quad (10)$$

$$\sum = \sum_{\nu_1 \geq \nu_2 \geq \nu_3 \geq \nu_4}^{n_1} \sum_{\nu_1}^{n_2} \sum_{\nu_2}^{m+\nu_1} (-)^{\nu_2 + \nu_1} (2\alpha)^{\nu_1 + \nu_1} C(\nu_4, \nu_3)$$

$$\times \binom{n_1}{\nu_1} \binom{n_2}{\nu_1} \binom{m+\nu_1}{\nu_2} \binom{\nu_1}{\nu_2} \binom{\nu_2}{\nu_3} \times \frac{(m+n_1)! (\nu_1+\nu_2)! \, \nu_4!}{(m+\nu_1)! (\nu_1+\nu_2-\nu_1+\nu_2)!}$$

$$\times \frac{(m+\nu_1+\nu_2+\nu_2-\nu_3)!}{(m+\nu_1+\nu_2)!} (2ik)^{\nu_1+\nu_4} \binom{i\beta+\nu_2}{\nu_2} \binom{-i\beta+m-1+\nu_1+\nu_4}{\nu_4}$$

$$\times q^{2\nu_4} \left[1 - (\hat{q} \cdot \hat{k})^2 \right]^{\nu_4} \times F \quad (11)$$

$$F = A^{-\nu_1-\mu_4} B^{-\nu_2-\mu_2} D^{\mu_2-\mu_4} D^{*\nu_1+\nu_2-\mu_1+\mu_2}$$

$$\times \left[-\frac{2(\alpha+ik)(m+\nu_1+\mu_4-i\beta)}{A} - \frac{2\alpha(1+\mu_2+\nu_2+i\beta)}{B} + \frac{\mu_2-\mu_4}{D} \right.$$

$$\left. + \frac{\nu_1+\nu_2-\mu_1+\mu_2}{D^*} \right] \qquad (12)$$

In these equations $\alpha = Z_e/na_o$, Z_e being the effective charge, $\beta = Z/ka_o$, where a_o is the Bohr radius and Z = 1 is the charge of the Coulomb field of the ejected electron, and A, B, and D are defined by

$$A = (\alpha+ik)^2 + q^2, \quad B = \alpha^2 + (\vec{q}-\vec{k})^2, \quad D = \alpha + i\hat{k}\cdot(\vec{q}-\vec{k}) \qquad (13)$$

The constants C (μ_4, μ_3) are given elsewhere.[10] ϕ_1 is the angle of azimuth of **q** with respect to **k** as the z-axis. The lower limits of all the demi variable integers in (11) are zero.

For evaluation of the second term on the right hand side of (7) we notice that $\langle k|n\ell m\rangle$ can be obtained by making $|\mathbf{q}|$ in the first term equal to zero. The second factor in this term can be evaluated by the usual methods; although the calculation is lengthy in algebra for large n values used here. The matrices in (7) involving **k** have been evaluated by taking the z-axis along **k**. Then the second term on the right hand side of (7) vanishes unless m = 0.

In this way the matrix in (1) is evaluated and $d\sigma/d(\epsilon/Ry)$ found accordingly. An integration of $d\sigma/d(\epsilon/Ry)$ with respect to ϵ/Ry will yield the total ionization cross section for ejection of an electron in a given atomic shell.

The effective charge for the atomic electron before ejection is found in the following way. Let Z be the atomic number of the atom, then the effective charge Z_e is given by $Z_e = Z - S$, where S is the screening parameter representing screening of the nucleus by other atomic electrons. S is defined by Hartree[11] through the relation $R = R_H/(Z - S)$ with R some linear scale of the atomic wave function under consideration, and R_H the corresponding value for the atomic hydrogen. It will be a good approximation to take R to be equal to the mean atomic radius $\bar{r}$. Froese[12] has assumed this to be the case, and gives S for several elements. We have used here values of S given by this author. For ionization of ions we have used the similar parameters given by Naqvi.[13] Effective charges and the ionization potentials of different atomic shells for the elements used here are given in Appendix I.

An examination of Eqs. (10) through (13) shows that the integrand on the right hand side of (1) depends only on q, k, and the angle between $\mathbf{q}$ and $\mathbf{k}$. Then for evaluation of (1) a two dimentional numerical integration, namely integration with respect to this angle and q, is necessary. An additional integration with respect to ϵ will give the total cross section.

In some measurements cross section per unit energy range of the ejected electron and per unit solid angle of the scattered electron is desirable. We give an expression for this quantity for the future use. Remembering the relationship between $\mathbf{q}$ and $\mathbf{k}_2$ we have that $qdq = k_1 k_2 d\Omega_2/(2\pi)$, where $d\Omega_2$ is the element of

the solid angle of the scattered particle with respect to the incident particle as the z-axis. From (1) the desired cross section is given by

$$\frac{\partial^2\sigma}{\partial\Omega_2\,\partial(\epsilon/R_y)} = \frac{2MZ'^2}{(2\ell+1)m_e a_o^3}\frac{\sqrt{\epsilon/R_y}}{E/R_y}\frac{k_1k_2}{q^4}\int\sum_{m=0}^{\ell}|\langle f|e^{i\vec{q}\cdot\vec{r}}|n\ell m\rangle|^2 d\hat{k} \qquad (14)$$

where the two dimensional angular integration is with respect to k_1 as the z-axis. While in (1) the integral is cyclic with respect to the angle of azimuth of $\mathbf{k}$, this is not the case here. If ϕ_2 and ϕ_k represent angles of azimuth of k_2 and k with respect to k_1 as the z-axis, the matrix in (14) contains terms with argument $(\phi_2 - \phi_k)$. This indicates that the left hand side of (14) is independent of ϕ_2.

For ionization of ions we have used plane wave for the incident, and Coulomb wave for the ejected, electrons. The use of the plane wave instead of the Coulomb wave for the incident particle is justifiable at high impact energies and the error incurred is of the same order as the error due to the use of the Born approximation. But the ejected electron wave function should always be described by a Coulomb wave.

For evaluation of the photoionization cross section we have used the well known formula[14]

$$\sigma_\nu = \frac{a_o^2 k\nu}{3c\,g_i}\left(\frac{2\pi}{a_o}\right)^3\sum_i\int|\langle\vec{k}|\vec{r}|i\rangle|^2 d\hat{k} \qquad (15)$$

in which ν is the frequency of the incident radiation, k the wave number of the ejected electron related to ν by the conservation of energy through $(2m_e)^{-1}\hbar^2 k^2 + I = h\nu$, I being the ionization potential of the ejected atomic electron. $|i\rangle$ is the eigenstate of the atomic electron and g_i its degeneracy number. $|\mathbf{k}\rangle$ is the Coulomb function of the atomic electron with normalization and effective charge described previously. $\hat{k}$ is a unit vector in the direction of k. It is seen that σ_ν has the dimension of length squared.

A relationship exists between photoionization cross section and the dipole approximation of the charged particle impact ionization. This can be obtained by expanding $\exp(i\mathbf{q}\cdot\mathbf{r})$ in (1), retaining the first non-vanishing term of the matrix, and employing (15). Then the differential cross section in the dipole approximation will be related to σ_ν through

$$\frac{d\sigma^D}{d(\epsilon/Ry)} = \frac{2}{\pi\alpha}\frac{MZ'^2}{m_e}\frac{R_y^2\sigma_\nu}{E(I+\epsilon)}\ln\frac{k_1+k_2}{k_1-k_2} \tag{16}$$

where $\alpha \cong 1/137$ is the fine structure constant of the Coulomb potential, and I is the ionization potential.

For small momentum transfer where the dipole approximation is valid we can write $k_1 + k_2 \cong 2k_1$, and $k_1 - k_2 \cong \Delta E/(2a_0^2 k_1 Ry)$, where $\Delta E = I + \epsilon$ is the excitation energy. In this way (16) reduces to

$$\frac{d\sigma^D}{d(\epsilon/Ry)} = \frac{2}{\pi\alpha}\frac{MZ'^2}{m_e}\frac{R_y^2\ln(4E/\Delta E)}{E\Delta E}\sigma_\nu\,, \tag{17}$$

giving the differential cross section in terms of the photoionization cross section σ_ν. Obviously $\nu = \Delta E/h$. In employing (17) note should be taken of the fact that σ_ν should correspond to low ejected electron energies, i.e., energies of the order of several threshold units, since the dipole approximation is valid for distant collisions, or low energy ejected electrons.

III. RESULTS AND DISCUSSION

The results of our calculations are presented in the following 23 figures. They are compared with the experimental data and with the results of some other representative quantum mechanical calculations.

The experimental data up to 1966 have been collected and reviewed in an article by Kieffer and Dunn.[15] Much of the experimental data used here has been taken from this review and referred to this reference accordingly.

In comparing the results of calculations with the experimental data note should be taken of the fact that in almost all measurements the quantity measured is the amount of ions produced. The measured ionic current I_T is given by

$$I_T = \sum n I^{n+} \tag{18}$$

where I^{n+} is the current due to the atoms which have lost n electrons. Some of the current is produced by direct collision and some is due to after collision processes such as autoionization or Auger effect.

There has been a number of measurements in which ions with specific charges on them, like singly or doubly charged ions, have been collected and measured. For all experiments mentioned in this paper all these measurements are relative while the measurement of the total ionic current given by (18) is absolute. Also, these measurements have less accuracy than the measurement of the total ionic current.

It then becomes obvious that in comparing calculation with measurement multiple ionization as well as autoionization should be taken into account. In the calculation reported here we have limited ourselves to single ionization from the individual shells only. Since the single ionization is the dominant process throughout the impact energy range, satisfactory agreement with experimental data is obtained in many cases. As an example, from the experimental evidence the production of singly charged ions from all shells at high impact energies accounts for 98% in helium, almost all in lithium, and 90% in neon, of the total ionic current. Then, for light elements up to neon we justifiably can compare our calculated cross section with measured total ionization cross section. For heavier elements this comparison is less justifiable due to the presence of many autoionization states.

In production of doubly charged ions four processes can take place. Three of these are double ionizations, simultaneous ionization and excitation, and double excitations. The latter two in certain cases may lead to the ejection of one for

the first case, and two for the second case, of additional electrons. The fourth process is a single inner shell ionization with subsequent cascading of the outer shell electrons and ejection of one or more electrons, called Auger electrons. Due to the large cross section of the single ionization compared to the multiple ionization, the fourth process at high impact energy is usually the dominant process compared to the other three. This is supported by the fact that our calculated cross section for single ionization of some inner shells almost equals the measured cross section for production of doubly charged ions in many cases.

We now give a description of the results.

A. Differential Cross Sections

Before giving a description of the total cross sections it is instructive and a critical test for the theory to present results for the calculated differential cross sections and a comparison with the experimental data available. By the differential cross section we mean here cross section per unit energy range of the ejected electrons. It will be a better test for the theory to compare cross sections per unit energy range of the ejected electron and per unit solid angle of the scattered electron with the experimental data, but this will not be done here. For the future use the formula for this cross section is given by (14).

In Fig. 1 the calculated differential cross sections for ionization of helium and neon by electron impact are given and compared with the recent measure-

ments of Opal, Peterson, and Beaty.[16] These are relative measurements normalized by the experimenters.

In the case of helium our calculation agrees fairly well with the experimental data except for the up turn seen at 50 eV in the experimental curve corresponding to the 100 eV primary energy. This up turn is most likely due to the exchange effect not taken into account in our calculation and which is important at the low impact energies.

In the case of neon the agreement is not as satisfactory as in the case of helium. In particular, the calculated curve seems to be flat in the region of low ejected electron energy. This is characteristic of the p-shell electron ionization in our model whose cross section dominates the neon, and also the carbon, nitrogen, and oxygen ionization differential cross sections to be discussed shortly.

In Fig. 2 the calculated differential cross section for ionization of helium by proton impact is given and compared with the measurements of Rudd, Sautter, and Bailey.[17] As can be seen the agreement is quite satisfactory. A more elaborate calculation on differential cross section for the ionization of helium by electron and proton impact with an accurate wave function has been done by Bell, Freeston, and Kingston.[18] The amount of agreement of the results of Bell et al with the data of Rudd et al is comparable to the agreement that we have found in our comparison with the data of Rudd et al. This indicates that a very accurate wave function is not necessary to calculate this differential cross section.

A similar test for the accuracy of the model employed here is a comparison of the measured and calculated photoionization cross sections. Using our data this comparison has been made for lithium by McDowell.[3] Here this comparison is reproduced and is shown in Fig. 3. The experimental data belongs to Hudson and Carter.[19] The calculated cross section is lower for low, and is higher for high, ejected electron energy compared to the experimental data.

B. Inert Gases

Our results for the inert gases are given in Figs. 4-9. For these gases we restrict ourselves chiefly to the calculation for production of singly charged ions. Source for all the experimental data, except those of Goudin and Hagemann,[20] and Schram,[21] is reference 15. It is seen that about the peak of the ionization curve, the experimental data are not consistent with each other, and they have considerable spread.

In the cases of helium, neon, and argon the experimental data displayed represent total experimental cross sections and are respectively about 2%, 10% and 12-15% higher than the observed single ionization cross sections in the energy range from 500 to several thousand eV.

In Figures 4, 5, 6 we have presented the results of our calculation and calculation of Peach.[4,22] For neon and argon our calculation clearly gives better agreement with experimental data than those of Peach.

For krypton and xenon (Figs. 7, 8, and 9) the data of Tate and Smith[23] are normalized to the multiple ion production measurements of Rapp and Golden at 400-500 and 500 eV, respectively (Cf. Ref. 15). Similarly, the data of Schram[21] are normalized to an earlier work of Schram, de Heer, Wiel and Kistemaker (Cf. Ref. 15).

For krypton it is seen that in their energy range the data of Schram complements those of Tate et al. T(4s + 4p) is our calculated curve, and as is seen at high impact energies, it is in reasonable agreement with the data of Schram.

For xenon (Fig. 8) the two measurements are in some disagreement with each other. Our calculation agrees better with measurement of Schram, and is somewhat higher than these measurements.

In Fig. 9 we compare our results for a single 3d shell ionization in krypton with the data of Tate and Smith[23] and Schram[21] for production of doubly charged ions in this element. We argue that the main source of the doubly charged ions at high impact energy is a single 3d shell ionization with a subsequent ejection of an Auger electron. Our results agree quite well with the high energy data of Schram. The disagreement with the data of Tate and Smith may be due to the production of doubly charged ions due to other processes important at low energies.

C. Alkalides

In Figures 10-14 ionization cross sections of alkalides ranging from lithium to cesium have been given. In Fig. 10 our results for both shell ionization clearly

gives better agreement with the absolute measurement of McFarland and Kinny[24] than the results of McDowell et al[28] marked MMP(2s). At high impact energies both calculated results seem to be lower than the results of measurements.

In Fig. 11 cross sections for production of singly and doubly charged sodium ions are presented. In accordance to what was said before production of the Na^{2+} ions is mainly due to the single ionization of the 2s shell and a subsequent Auger process. This is confirmed by the fact that $\sigma(2s)$ which gives cross section for the ejection of a 2s electron shown in the figure by T(2s) is in agreement with cross section for the production of doubly charged ions.

In Figs. 12-14 ionization of potassium, rubidium, and cesium are presented. T(3s), T(4s), and T(5s) in the three figures represent twice the calculated cross sections for single ionization of the inner s-shell electrons, since these single ionizations give rise to doubly charged ions. In these figures the experimental curves for the production of doubly charged ions have lower thresholds compared to T(3s), T(4s), and T(5s) curves. Also, they give larger cross sections at low impact energies. This can partially be explained by the importance of autoionization at low energies. In particular, autoionizations permit formation of doubly charged ions below the threshold of the inner s shell electrons. At higher energies autoionization is probably not as important and the Coster-Kronig type Auger electrons can account for the majority of the doubly charged ions.

It should be emphasized that the experimental curves in Figs. 10-14, unless otherwise specified, are for production of the total ionic current. While the production of ions with charge greater than two is negligible for Li, Na, and K, Tate and Smith[23] have shown that at 500 eV 13% for rubidium and 18% for cesium of the total ionic current are due to triply or higher charged ions. Thus in comparing the experimental data of McFarland and Kinney with our total cross sections T(4s+4p+5s) for Rb and T(5s+5p+6s) for Cs an appropriate reduction in their cross sections should be made, but this has not been done here.

It will be interesting to notice how the results of McFarland and Kinney, which are most recent, absolute, and are extended to high impact energies, compare to our results for the five alkalides given in Figs. 10-14. It is noticed that for Li, Na, and Cs the experimental values lie above, and for K and Rb they lie below, the theoretical results. Although we have employed a crude model for calculation, no consistent discrepancy is found with measurements. More refined calculation should give better agreement with measurements.

There seems difficulty in reconciling our results with the data of Tate and Smith for high energy ionization of Rb and Cs (Cf. Figs. 13 and 14) as is seen in the "flattening" of the curves due to these data. Similarly, as is seen in Figs. 13 and 14, while the T(5s) curve representing single 5s ionization correctly gives the production of doubly charged cesium ions, the T(4s) curve does not give the production of the doubly charged rubidium ions. To resolve the differences, and

since the measurement of Tate and Smith is 36 years old, a new measurement for the relevant cases is desirable.

The irregular variation in the ion production in K, Rb, and Cs at low impact energy is due to numerous autoionizing states in these atoms which has not been taken into account in our calculations.

D. Magnesium and Zinc

In Figures 15 and 16 our results for ionization of magnesium and zinc are shown. As is seen in Fig. 15 our calculated curve marked T(3s) for single ionization of magnesium is in fair agreement with the measurement at high impact energies, but near the peak calculated results are substantially lower than the measurement. Measurements of Kaneko[34] (not shown in the figure) indicate the presence of a number of autoionization lines from threshold up to the peak of the ionization curve.

In Fig. 15 it is also seen that the cross section for production of doubly charged ions compared to singly charged ions in magnesium is much larger than the same quantity for sodium. While for sodium the doubly charged current accounts for only 10% of the total cross section at high ernergies, in magnesium it is 50%. The difference is most likely due to the fact that in Mg the ejection of a 2p electron can be followed by the emission of a 3s electron through the Auger process. This cannot take place in sodium since the energy gap between 2p and 3s in sodium is not wide enough to make the process operational, and also due to the fact that there is only one 3s electron in sodium.

In Fig. 15 the curve Mg^{2+} lies higher than the calculated curve T(2s+2p) which is assumed to give the cross section for the Auger process. The discrepancy may be due to a number of reasons and cannot be explained easily.

Figure 16 gives calculated cross sections for ejection of 4s, 3d, and 3p electrons in zinc. No measurement on ionization of zinc is available. Photoionization data on Zinc[35] indicate that the element is rich in autoionization states at the low energy side of the peak of the ionization cross section. We then anticipate that the peak in the measured ionic current will be higher than the peak of the curve marked T(3p+3d+4s). As usual we have assumed that 3p shell electron ionization will lead to the production of doubly charged ions through the Auger process. For this reason σ(3p) has been multiplied by a factor of 2 before being added to the cross section for the total ionic current marked by T(3p+3d+4s).

The shape of the curve found by Fiquet-Fayard et al[36] for production of Zn^{++} (not shown in the figure) is similar to T(3p) above 500 eV. Since the cross section as a function of energy at high impact energy according to the T(3p) curve is given as $E^{-1}(A\ln E + B)$ with A and B constants, the similarity suggests that Zn^{++} production at high energy is dominated by the Auger process due to single ionization. At lower energies other processes should be taken into account. This would probably make the curve for the production of Zn^{++} to lie higher than T(3p) at low energies.

Because of the small size of the Fiquet-Fayard figures, their reproduction is difficult and is not done here.

E. Carbon, Nitrogen, and Oxygen

Figs. 17-19 gives our results for single ionization of carbon, nitrogen and oxygen. No experimental data is available for carbon. For nitrogen and oxygen the experimental data are in as much disagreement with each other as are different calculations.

It is important to note that in these three elements contribution to the ionization cross section of the 2s shell is almost as important as the 2p shell, and in any calculation the two shells should be taken into account. The earliest calculation due to Seaton, S(2p) in the figure, contains contribution of the 2p shell only.

In Figs. 20-22 cross sections per unit energy range of the ejected electrons for electron impact ionization of carbon, nitrogen, and oxygen are given. Because of the abundance of these elements in the atmosphere and other parts of the cosmos, these cross sections will be useful for a number of problems related to the stopping power of the atmospheric and cosmic gases. The agreement found in Fig. 1 indicates the likelihood of the accuracy of the differential cross sections given in Figures 20-22.

F. Ionization of Ions

In the ionization of ions the incident particle should be described by a Coulomb wave function. At high impact energies the Coulomb wave can be replaced by a

plane wave. It can be shown that the resultant inaccuracy is comparable to the inaccuracy in the Born approximation. This has been verified by Peart, Walton, and Dolder[38] who have compared their absolute cross section measurement of electron impact ionization of He^+ with a Born calculation where a plane wave is used for the incident electron.

Here we apply our model to the ionization of a non-hydrogenlike ion, namely Li^+. Effective charge and ionization potential of Li^+ necessary in our calculation is given in the Appendix.

In Figure 23 we have constructed a Bethe plot for ionization of Li^+ by electron impact. Measured cross sections are by Peart et al (opt. cit.), and by Peart and Dolder.[39] The measurement is well extended into the relativistic region. When the projectile has relativistic energies, the target, excluding the inner shell of heavy atoms and ions, can still be treated non-relativistically. The relativistic correction for the projectile has been made by Bethe.[40] The non-relativistic high energy inelastic atomic cross section according to Bethe[41] is given by $\sigma = E^{-1}$ (A ln E + B) with E the relative kinetic energy of the system, and A and B some atomic constants. For relativistic projectiles this expression should be replaced by

$$\left(\frac{1}{2} m v^2\right) \sigma = A \left\{ \ln \left[\frac{1}{2} m v^2 / (1-\beta^2) \right] - \beta^2 \right\} + B \qquad (19)$$

with m and v the rest mass and velocity of the projectile, $\beta = v/c$, c being the speed of light, and A and B the non-relativistic atomic constants.

In Fig. 23 the straight line R is a plot of the left hand side versus the expression in the curly bracket in (19). The slope and the intersection of R gives A and B. It has been obtained by constructing a segment of R in the non-relativistic high energy region, using for σ the computed Born cross section. By extension of the segment R has been obtained. The curve NR has been obtained by using for σ the computed Born cross section throughout the range of the curve. The departure of NR from R curve at high impact energy is a measure of the amount of the relativistic correction.

If the relativistic correction were not necessary the experimental points should fall on NR curve, assuming the accuracy of our non-relativistic calculation. With relativistic correction the experimental data should agree with R. Although the experimental data are extended to the relativistic region because of their error bars the correctness of the relativistic correction cannot be verified, and this verification is left to the future.

Before closing this section we make three remarks. It is of interest to know the relative contribution of different atomic shells to the ionization cross section. There is no simple quantum mechanical expression for this relative contribution, but an order of magnitude relation can be obtained using the Thomson's classical formula for ionization. According to this formula the ratio of the cross sections

Q_1^c and Q_2^c for two elements 1 and 2 evaluated at equal threshold units of energies is given by[43]

$$Q_2^c / Q_1^c = (I_1 / I_2)^2 \qquad (20)$$

where I_1 and I_2 are the ionization potentials of the two elements. Thus, as the ionization potentials of the inner shells get larger, ionization cross section of these shells get smaller, approximately as the inverse square of the ionization potentials. Contribution of the inner shell ionization in many cases can then be neglected.

A second remark is about construction of the Bethe plot for many electron atom ionization. Since high energy non-relativistic cross section is given by $\sigma = E^{-1} (A \ln E + B)$, a plot, called the Bethe plot, of $E\sigma$ versus $\ln E$ falls on a straight line. For heavy elements when the incident energy has reached many times the ionization potential of the outer shell electrons, corresponding to the validity of the above expression, the energy may not have reached the threshold energy of the inner shell electrons. Thus construction of Bethe curves for heavy elements in the energy range of interest is not possible. For lighter elements this is possible, and the two parameters of the curve give all the necessary information for the high impact energy total cross sections.

Finally, we have established that Auger transition in production of doubly charged ions is a dominating process. This is supported by the present calculation which shows that for several elements the inner shell ionization responsible

for the Auger transition yields cross sections very close to that observed for the production of doubly charged ions. In addition, Schram et al[21,44] and Fiquet-Fayard et al[36] have shown that cross section for this production behaves as $E^{-1}(A \ln E + B)$ with A and B comparable to each other in their magnitudes. Since in multiple ionization or excitation A is very small compared to B, our assumption is verified. The cases of K and Rb may however be exceptions as the measurement of Fiquet-Fayard et al above 500 eV indicates that the cross section for production of K^{++} and Rb^{++} (not shown in the figures) falls off faster as a function of energy than the curves T(3s) and T(4s) in Figs. 12 and 13 indicate. The discrepancy may be due to a number of reasons which we will not discuss here.

IV. CONCLUSION

1. By the use of a simple model we have calculated a number of ionization cross sections in fair agreement with measurements. Its simplicity and relative accuracy makes it a useful calculational tool for further ionization calculations. We also have shown that the model can be used for ionization of ions with an accuracy comparable to the atomic ionization.

2. In comparing our results with the experimental data for differential ionization cross sections we have found that agreement is comparable to the agreement of the more sophisticated calculations with accurate wave functions We conclude that the accuracy of the differential ionization cross section is not very sensitive to the accuracy of the wave functions.

3. We have shown that in a number of elements production of doubly charged ions is mainly due to Auger processes whose cross section is given by certain inner shell ionization cross sections.

FIGURE CAPTIONS

Fig. 1. Cross section per unit energy range of ejected electrons in ionization of helium and neon by electron impact. The energy of the primary in eV is marked on each curve. The measurements are due to Opal, Peterson, and Beaty (Ref. 16).

Fig. 2. Cross section per unit energy range of ejected electrons in ionization of helium by proton impact. The experimental data are due to the absolute measurement of Rudd, Sautter, and Bailey (Ref. 17).

Fig. 3. Photoionization of lithium. Measurement of Hudson and Carter (Ref. 19) is compared with our calculation.

Fig. 4. Ionization of helium by electron impact. In this and all the following figures through Fig. 19, and Fig. 22, σ is the ionization cross section in units of πa_o^2, and E is the impact energy in units of eV. All the experimental data in this figure and the following two figures are absolute measurements. For a description see Ref. 15, except the data of Gaudin and Hagemann which is described in Ref. 20. The two solid lines are calculations of Peach (Ref. 22), and ours.

Fig. 5. Ionization of neon by electron impact. See Refs. 15 and 20 for a description of the measurements. T(2p), T(2s), and T(2s + 2p) represent present calculations and give $\sigma(2p)$, $\sigma(2s)$, and the sum of $\sigma(2p)$ and $\sigma(2s)$, respectively. P(2s + 2p) is calculation of Peach (Ref. 4) and gives the sum of $\sigma(2p)$ and $\sigma(2s)$ plus autoionization.

Fig. 6. Ionization of argon by electron impact. See Refs. 15 and 20 for a description of the measurements. T(3p), T(3s), and T(3s + 3p) represent the present calculations and they give $\sigma(3p)$, $\sigma(3s)$ and the sum of $\sigma(3p)$ and $\sigma(3s)$ respectively. P(3p) and P(3s) are calculations of Peach (Ref. 4) and they give $\sigma(3p)$ and $\sigma(3s)$, respectively. In P(3s) autoionization has also been taken into account.

Fig. 7. Single ionization of krypton by electron impact. Kr^+ curve gives the measured cross section for production of Kr^+. The relative measurements of Tate and Smith (Ref. 23), and Schram (Ref. 21) are normalized as described in the text. T(4p), T(4s), and T(4s + 4p) represent the present calculations and they give $\sigma(4p)$, $\sigma(4s)$, and the sum of $\sigma(4p)$ and $\sigma(4s)$, respectively.

Fig. 8. Single ionization of xenon by electron impact. Xe^+ gives relative measured cross section for production of singly charged xenon ions. See Fig. 7 for references. T(5p), T(5s), and T(5s + 5p) represent the present calculations and give $\sigma(5p)$, $\sigma(5s)$ and the sum of $\sigma(5p)$ and $\sigma(5s)$, respectively.

Fig. 9. Production of doubly charged krypton ions by electron impact. Kr^{++} curve gives twice the relative measured cross section for production of doubly charged ions, see Fig. 7 for references. Present calculation gives $2\sigma(3d)$ with $\sigma(3d)$ the cross section for single ionization of a 3d shell electron. The colliding atom becomes doubly ionized by subsequent ejection for an Auger electron.

Fig. 10. Ionization of lithium by electron impact. Measurements of McFarland and Kinney (Refs. 15, 24, 25), and Zapesochnyi and Aleksakhin (Ref. 26) are absolute total experimental cross sections; those of Brink (Ref. 27) are relative normalized to the results of McFarland et al. The two curves marked T are the present calculations; one for ionization of the outer shell, and the other for ionization of both inner and outer shells of lithium. MMP(2s) is the outer shell calculation of McDowell et al (Refs. 3, 28).

Fig. 11. Ionization of sodium by electron impact. Measurements of McFarland and Kinney (Refs. 15, 24, 25), and Zapesochnyi and Aleksakhin (Ref. 26) are absolute total experimental cross sections. Those of Tate and Smith (Ref. 23), and Brink (Ref. 27) are the cross sections for the production of the ions Na^+ and Na^{2+}. They are relative and are normalized at 500 eV to the results of McFarland and Kinney. Curves marked

by T represent the present calculation. T(3s) gives $\sigma(3s)$, 3s being the outermost shell, T(2s) gives $2\sigma(2s)$, and T(2p+3s) gives the sum of $\sigma(3s)$ and $\sigma(2p)$ and is to be compared to the experimental Na^+ curves. T(2s+2p+3s) gives the sum of $\sigma(3s)$, $\sigma(2p)$ and $2\sigma(2s)$, and must be compared with the measured total ionization cross section. For an explanation see the text. BBP(3s) is calculation of Bates et al (Ref. 29) for $\sigma(3s)$, and P(2p+3s) is calculation of Peach (Ref. 4) for the sum of $\sigma(3s)$ and $\sigma(2p)$.

Fig. 12. Ionization of potassium by electron impact. The measurement of Korchevoi and Prozonski (Ref. 30) is absolute. For other measurements see Fig. 11. T curves represent the present calculations, T(4s), T(3p) and T(3s) gives $\sigma(4s)$ and $\sigma(3p)$, and $2\sigma(3s)$, respectively. T(3p+4s) gives the sum of $\sigma(4s)$ and $\sigma(3p)$, and is to be compared with the experimental curves for K^+, and T(3s+3p+4s) gives the sum of $\sigma(4s)$, $\sigma(3p)$, and $2\sigma(3s)$ and is to be compared with the total experimental cross sections of McFarland and Kinney.

Fig. 13. Ionization of rubidium by electron impact. For explanation of measurements see Fig. 12. T curves represent the present calculations. T(5s), T(4p), and T(4s) give $\sigma(5s)$, $\sigma(4p)$, and $2\sigma(4s)$, respectively. T(4p+5s) gives the sum of $\sigma(5s)$ and $\sigma(4p)$, and is to be compared with the Rb^+ curve of Tate and Smith. T(4s+4p+5s) gives the sum of $\sigma(5s)$, $\sigma(4p)$, and $2\sigma(4s)$ but in this case it should be smaller than the total experimental cross sections of McFarland and Kinney, see text.

Fig. 14. Ionization of cesium by electron impact. For measurement of Heil and Scott see Ref. 31. For other measurements see Fig. 12. T curves represent the present calculations. T(6s), T(5p), and T(5s) give $\sigma(6s)$, $\sigma(5p)$, and $2\sigma(5s)$, respectively. T(5p+6s) gives the sum of $\sigma(6s)$ and $\sigma(5p)$ and should be compared with the measurement for Cs^+. T(5s+5p+6s) gives the sum of $\sigma(6s)$, $\sigma(5p)$, and $2\sigma(5s)$ and should be compared to the total experimental cross sections of McFarland and Kinney, see text.

Fig. 15. Ionization of magnesium by electron impact. Mg^+ and Mg^{++} curves gives cross sections for production of singly and doubly charged ions; cross section for the latter curve being multiplied by a factor of 20. The measurement of Okuno et al (Ref. 32) is the absolute total ionization cross section. The relative measurements of Okudaira et al (Ref. 33) were normalized by the experimenters at 500 eV to the results of Okuno et al. T curves represent the present calculations. T(3s), T(2s + 2p), and T(2s + 2p + 3s) give $\sigma(3s)$, $20\,[\sigma(2p) + \sigma(2s)]$, and $\sigma(3s) + 2\sigma(2p) + 2\sigma(2s)$, respectively. P(3s) and P(2p) are calculations of Peach (Ref. 4). They give $\sigma(3s)$ and $20\sigma(2p)$, respectively. In P(2p) curve the autoionization has also been taken into account, accounting for its dip.

Fig. 16. Ionization of zinc by electron impact. T curves represent the present calculations. T(4s), T(3d), and T(3p) give $\sigma(4s)$, $\sigma(3d)$, and $40\sigma(3p)$, respectively. T(3d + 4s) is the sum of $\sigma(4s)$ and $\sigma(3d)$, and T(3p + 3d + 4s) is the sum of $\sigma(4s)$, $\sigma(3d)$, and $2\sigma(3p)$.

Fig. 17. Ionization of carbon by electron impact. T(2p), T(2s), and T(2s + 2p) represent the present calculations and give $\sigma(2p)$, $\sigma(2s)$, and the sum of $\sigma(2p)$ and $\sigma(2s)$. No measurement is available on ionization of this element

Fig. 18. Ionization of atomic nitrogen by electron impact. Measurement of Smith et al is for total ionic current while that of Peterson is for N^+ current. For a description of the experimental results see Ref. 15. T(2p), T(2s), and T(2s + 2p) represent the present calculations and give $\sigma(2p)$, $\sigma(2s)$, and the sum of $\sigma(2p)$ and $\sigma(2s)$. P(2s + 2p) is calculation of Peach (Ref. 4) for the sum of $\sigma(2p)$ and $\sigma(2s)$ plus autoionization.

Fig. 19. Ionization of atomic oxygen by electron impact. Measurement of Fite et al and Bokesenberg is for O^+ production while that of Rothe et al is for total ion production. For a description see Ref. 15.

T(2p), T(2s), and T(2s + 2p) represent the present calculations and give $\sigma(2p)$, $\sigma(2s)$, and the sum of $\sigma(2p)$ and $\sigma(2s)$ respectively. S(2p) is calculation of Seaton (Ref. 37) for $\sigma(2p)$.

Fig. 20. Cross section per unit energy range of ejected electrons in ionization of carbon by electron impact. The energy of the primary is marked on each curve.

Fig. 21. Cross section per unit energy range of ejected electrons in ionization of nitrogen by electron impact. The energy of the primary is marked on each curve.

Fig. 22. Cross section per unit energy range of ejected electrons in ionization of oxygen by electron impact. The energy of the primary is marked on each curve.

Fig. 23. Ionization of lithium ion by electron impact. The experimental cross section for production of Li^{++} is due to the absolute measurement of Peart, Walton, and Dolder (Ref. 38), and Peart and Dolder (Ref. 39). R represents our calculation with relativistic correction. NR is our non-relativistic Born calculation. Presented also are calculations of Moores and Nussbaumer (Ref. 42) shown by MN curve in the figure. For other calculations see Ref. 38.

REFERENCES

1. G. H. Wannier, Phys. Rev. 90, 817 (1953)

2. L. Vriens, Case Studies in Atomic Collison Physics I, Eds. E. W. McDaniel and M. R. C. McDowell (North Holland Publishing Co., 1969), Ch. 6

3. M. R. C. McDowell, Opt. Cit., CH. 2

4. G. Peach, J. Phys. B, 3, 328 (1970)

5. E. J. McGuire, Phys. Rev. 3, 267 (1971)

6. Some of the results presented here are given by K. Omidvar and E. C. Sullivan, Bulletin of the 5th International Conference of the Physics of Electronic and Atomic Collisions (Publishing House Nauka, Lenningrad, USSR, 1967) p. 452

7. E. H. S. Burhop, Proc. Camb. Phil. Soc. 36, 43 (1940)

8. A. O. Barut and H. Kleinert, Phys. Rev. 160, 1149 (1967)

9. J. W. B. Hughes, Proc. Phys. Soc. (London) 91, 810 (1967)

10. K. Omidvar, Phys. Rev. 140, A26 (1965), Table I

11. D. R. Hartree, Proc. Camb. Phil. Soc. 51, 684 (1955)

12. C. Froese, J. Chem. Phys. 45, 1417 (1966). Also, C. Froese, Hartree-Fock Parameters for the Atoms Helium to Radom, Technical Note, Department of Mathematics, University of British Columbia, Vancouver 8, B. C., Canada

13. A. M. Naqvi, J. Quant. Spectroscopy and Radiation Transfer, 4, 597 (1964). Also, A. M. Naqvi and G. A. Victor, Calculations of Wave Functions and Transition Probabilities, Technical Document Report RTD TDR-63-3118, Air Force Weapons Laboratory, Kirkland Air Force Base, New Mexico

14. H. A. Bethe, Intermediate Quantum Mechanics (W. A. Benjamin, Inc., New York, 1964), Ch. 14

15. L. J. Kieffer and G. H. Dunn, Rev. Mod. Phys. 38, 1 (1966)

16. C. B. Opal, W. K. Peterson, and E. C. Beaty, Bull. of Am. Phys. Soc., 15, 1522 (1970), and private communication

17. M. E. Rudd, C. A. Sautter and C. L. Bailey, Phys. Rev. 151, 20 (1966)

18. K. L. Bell, M. W. Freeston, and A. E. Kingston, J. Phys. B, 3, 959 (1970)

19. R. D. Hudson and V. L. Carter, J. Opt. Soc. Am. 57, 651 (1967)

20. A. Goudin and R. Hagemann, J. Chim. Phys. 64, 1209 (1967)

21. B. L. Schram, Physica 32, 197 (1966)

22. G. Peach, Proc. Phys. Soc. (London) 85, 709 (1965)

23. J. T. Tate and P. T. Smith, Phys. Rev. 46, 773 (1934)

24. R. H. McFarland and J. D. Kinney, Phys. Rev. 137, A1058 (1965). Cross sections for single ionization of sodium, rubidium, and cesium given in this reference are in error. For corrected values see Ref. 25.

25. R. H. McFarland, Phys. Rev. 139, A40 (1965)

26. I. P. Zapesochnyi and I. S. Aleksakhin, Soviet Physics JETP, 28, 41 (1969) [Translated from Zh. Eksp. Teor. Fiz. 55, 76 (1968)]

27. G. O. Brink, Phys. Rev. 127, 1204 (1962)

28. M. R. C. McDowell, V. P. Myerscough, and G. Peach, Proc. Phys. Soc. (London) 85, 703 (1965)

29. D. R. Bates, A. H. Boyd, and S. S. Prasad, Proc. Phys. Soc. (London) 85, 1121 (1965)

30. Y. P. Korchevoi and A. M. Prozonski, Soviet Physics JETP 24, 1089 (1967) [Translated from Zh. Eksp. Teor. Fiz. 51, 1617 (1966)]

31. H. Heil and B. Scott, Phys. Rev. 145, 279 (1966)

32. Y. Okuno, K. Okuno, Y. Kaneko, and I. Kanomata, J. Phys. Soc. (Japan) 29, 164 (1970)

33. S. Okudaira, Y. Kaneko, and I. Kanomata, J. Phys. Soc. (Japan) 28, 1536 (1970)

34. Y. Kaneko, J. Phys. Soc. (Japan) 16, 2288 (1961)

35. G. V. Marr and J. M. Austin, J. Phys. B 2, 107 (1968)

36. F. Fiquet-Fayard, J. Chiari, F. Muller, and J. P. Ziesel, J. Chem. Phys. 48, 478 (1968)

37. M. J. Seaton, Phys. Rev. 113, 814 (1959)

38. B. Peart, D. S. Walton and K. T. Dolder, J. Phys. B 2, 1347 (1969)

39. B. Peart and K. T. Dolder, J. Phys. B 1, 872 (1968)

40. N. F. Mott and H. S. W. Massey, The Theory of Atomic Collisions, 3rd Edition (Oxford: Clarendon Press, 1965) p. 815

41. H. A. Bethe, Ann. Physik 5, 325 (1930)

42. D. L. Moores and H. Nussbaumer, J. Phys. B 3, 161 (1970)

43. See for example M. R. H. Rudge, Rev. Mod. Phys. 40, 564 (1968)

44. B. L. Schram, A. J. H. Boerboom, and J. Kistemaker, Physica 32, 185 (1966)

Appendix I

Values of the Effective Charges Z_e and the Ionization Potentials IP Employed[a]

Atomic Number	Element	Shell	Ze	IP (eV)	Atomic Number	Element	Shell	Ze	IP (eV)
2	He	1s	1.618	24.580	19	K	4s	4.577	4.339
							3p	8.700	24.63
3	Li	2s	1.549	5.39			3s	10.571	40.8
		1s	2.617	67.407					
					30	Zn	4s	8.282	9.391
6	C	2p	2.869	11.264			3d	12.002	17.4
		2s	3.784	19.375			3p	17.366	93.4
7	N	2p	3.456	14.54	36	Kr	4p	11.785	13.996
		2s	4.524	20.325			4s	14.730	27.6
							3d	19.06	96.86
8	O	2p	4.035	13.614					
		2s	5.260	28.44	37	Rb	5s	6.659	4.176
							4p	13.257	21.16
10	Ne	2p	5.180	21.599			4s	16.009	34.74
		2s	6.726	47.5					
					54	Xe	5p	15.612	12.127
11	Na	3s	3.208	5.138			5s	18.930	23.4
		2p	6.262	38.094					
		2s	7.702	70.75	55	Cs	6s	8.564	3.893
							5p	17.289	17.859
12	Mg	3s	4.150	7.644			5s	20.387	28.14
		2p	7.299	58.2					
		2s	8.691	96.2	3	Li^+	1s	2.683	75.282
18	Ar	3p	7.517	15.755					
		2s	9.493	29.24					

[a]The effective charge for atoms were taken from Ref. 12, and for Li^+ from Ref. 13. All outer shell ionization potentials were taken from M. A. Lange in the Handbook of Chemistry, 10th Ed. (McGraw Hill, Inc., New York, N.Y., 1961) p. 111. The inner shell ionization potentials were taken from the available photo ionization data (Cf. R. D. Hudson and L. J. Kieffer, JILA Information Report No. 11, JILA, U. of Colorado, Boulder, Colorado, 1970). In other cases energy levels based on X-ray data were used (Cf. J. C. Slater, Phys. Rev. 98, 1039 (1955), and J. A. Beardon and A. F. Burr, Rev. Mod. Phys. 39, 125 (1967))

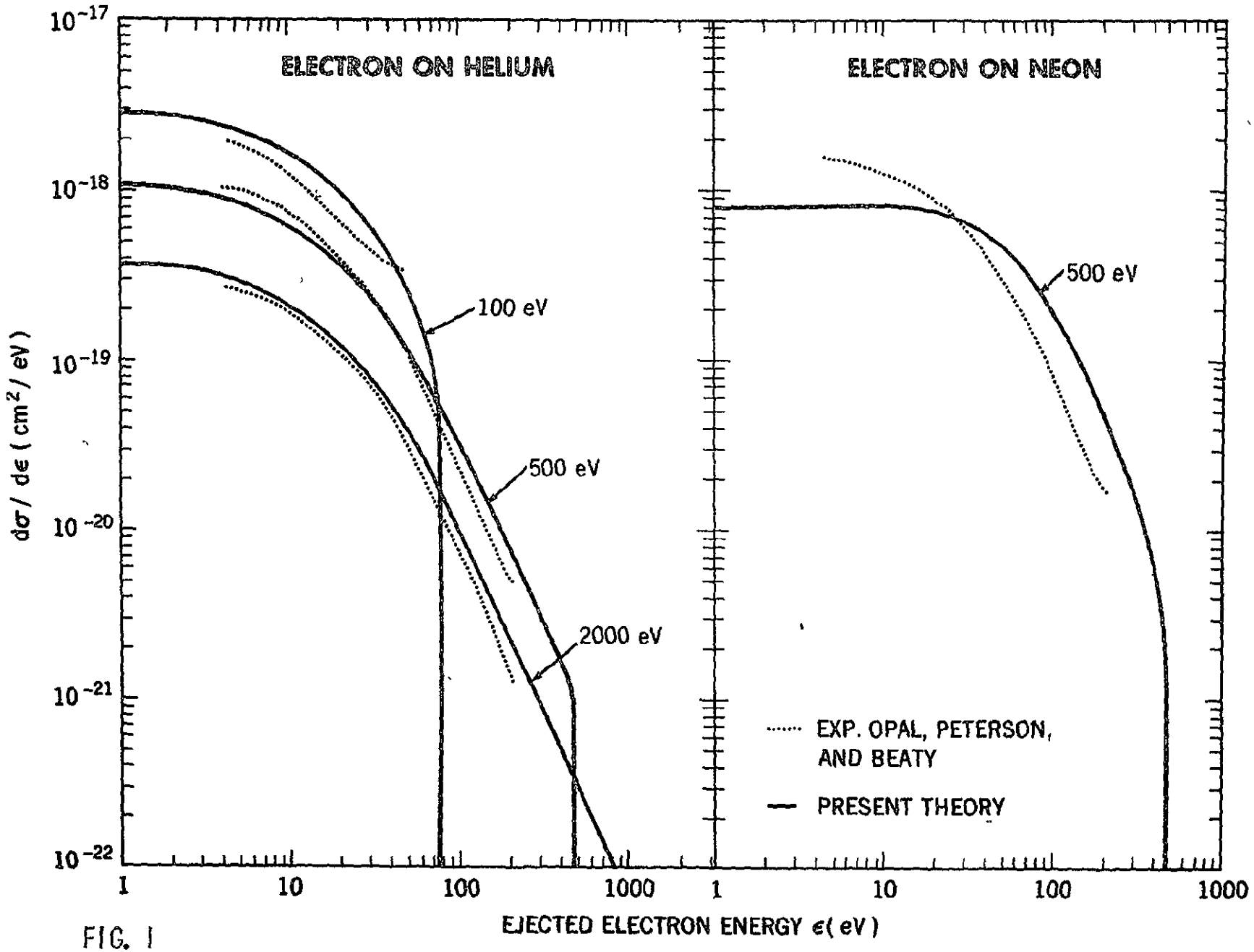
ELECTRON ON HELIUM
ELECTRON ON NEON
100 eV
500 eV
2000 eV
500 eV
EXP. OPAL, PETERSON, AND BEATY
PRESENT THEORY
dσ/dε (cm²/eV)
EJECTED ELECTRON ENERGY ε(eV)
10⁻¹⁷
10⁻¹⁸
10⁻¹⁹
10⁻²⁰
10⁻²¹
10⁻²²
1
10
100
1000

FIG. 1

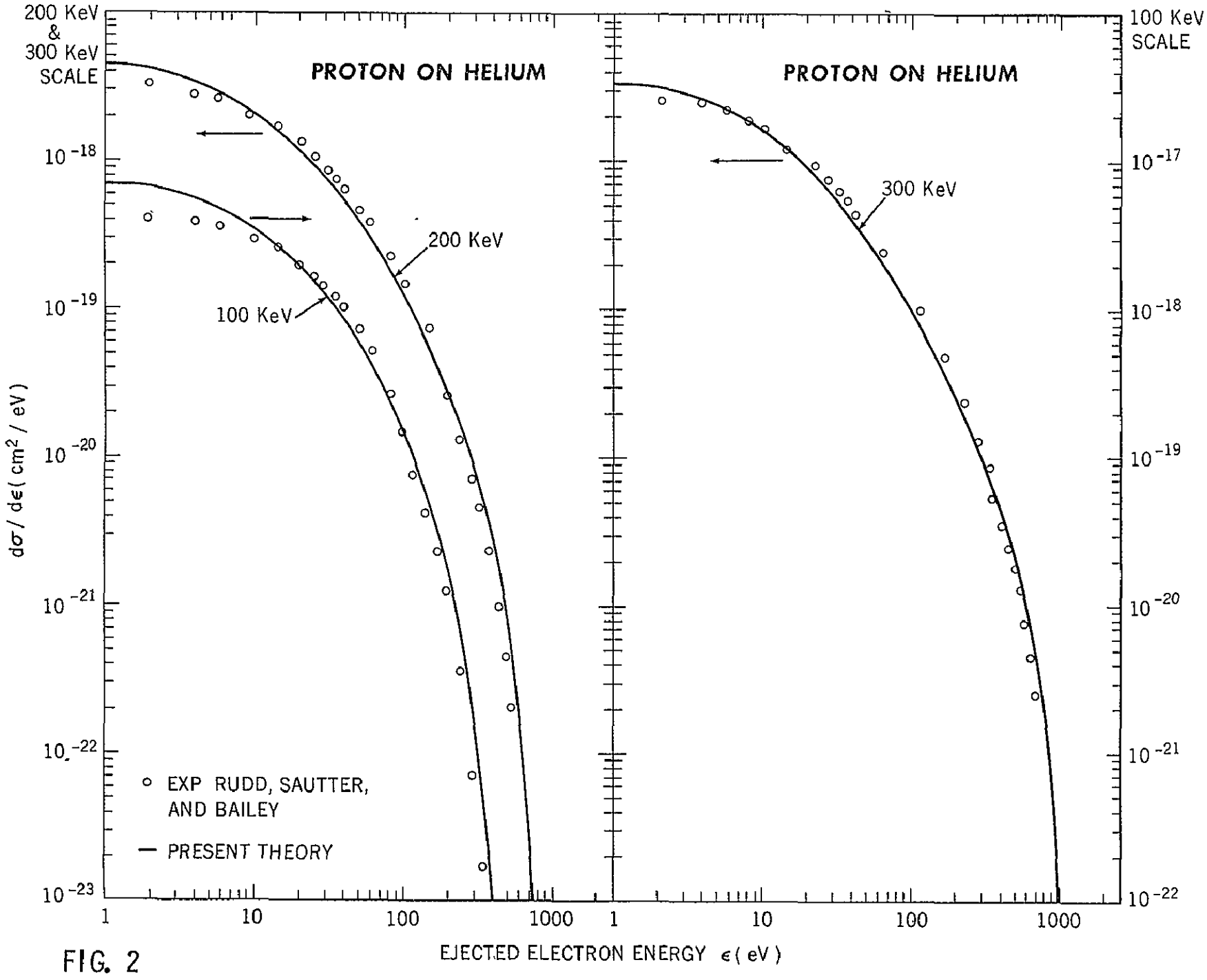
200 KeV
&
300 KeV
SCALE
PROTON ON HELIUM
200 KeV
100 KeV
100 KeV
SCALE
PROTON ON HELIUM
300 KeV
10^{-18}
10^{-19}
10^{-20}
10^{-21}
10^{-22}
10^{-23}
10^{-17}
10^{-18}
10^{-19}
10^{-20}
10^{-21}
10^{-22}
$d\sigma / d\epsilon$ (cm^2 / eV)
EXP RUDD, SAUTTER, AND BAILEY
PRESENT THEORY
1
10
100
1000
1
10
100
1000
EJECTED ELECTRON ENERGY ϵ (eV)

FIG. 2

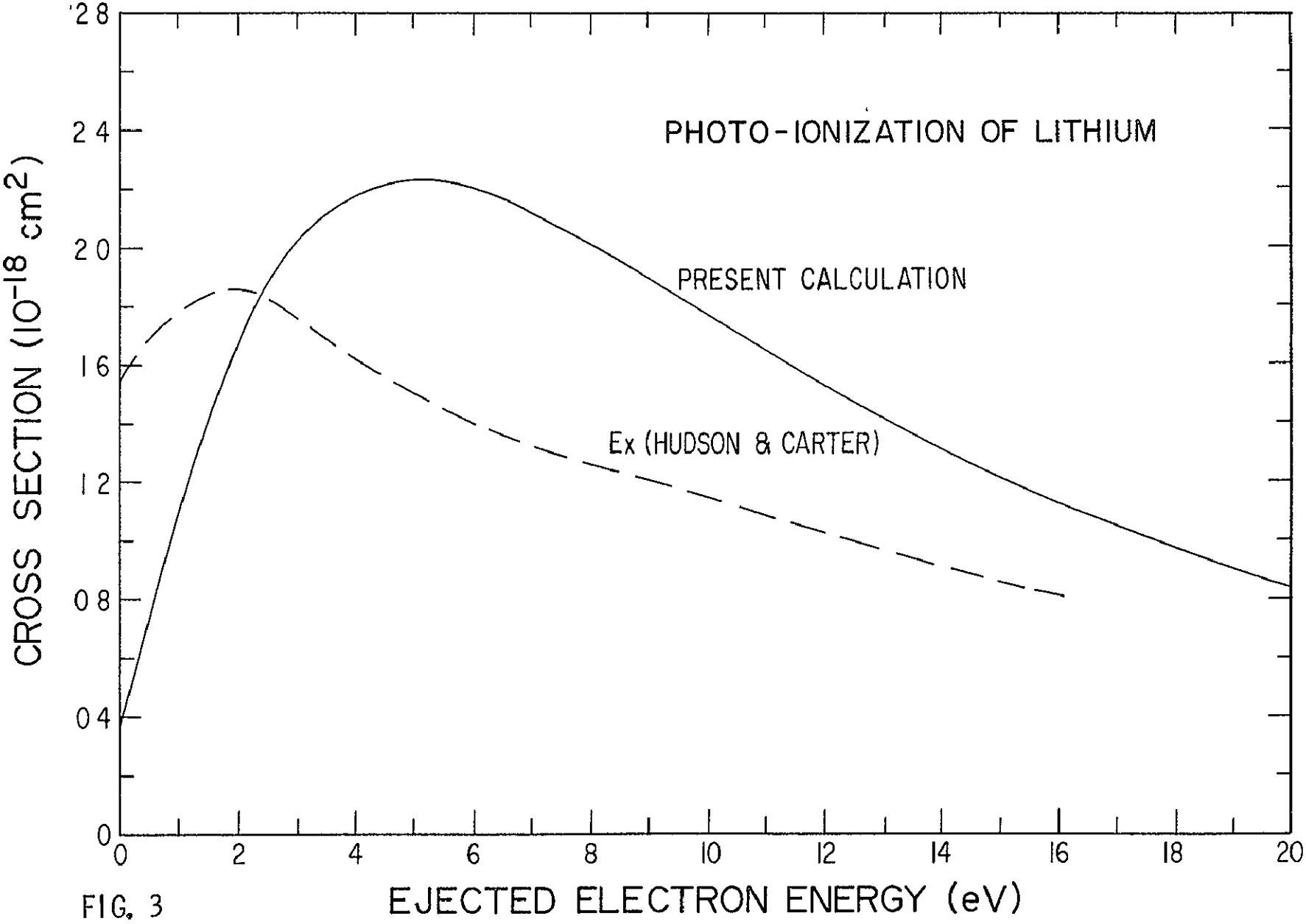
PHOTO-IONIZATION OF LITHIUM
PRESENT CALCULATION
Ex (HUDSON & CARTER)
CROSS SECTION (10^{-18} cm^2)
EJECTED ELECTRON ENERGY (eV)
0
0 4
0 8
1 2
1 6
2 0
2 4
2 8
0
2
4
6
8
10
12
14
16
18
20

FIG. 3

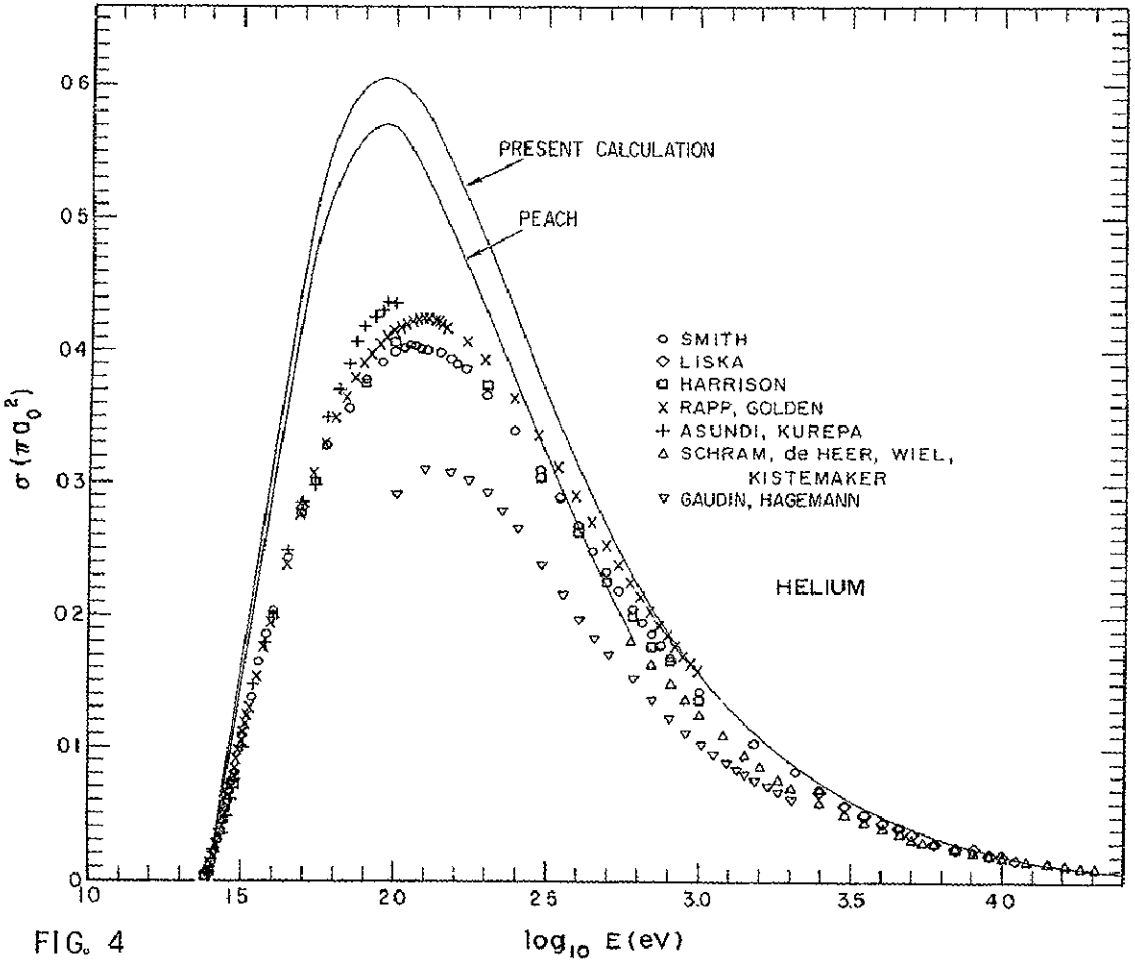
PRESENT CALCULATION
PEACH
SMITH
LISKA
HARRISON
RAPP, GOLDEN
ASUNDI, KUREPA
SCHRAM, de HEER, WIEL, KISTEMAKER
GAUDIN, HAGEMANN
HELIUM
σ (πa0²)
0
01
02
03
04
05
06
10
15
20
25
3.0
3.5
40
log10 E (eV)

FIG. 4

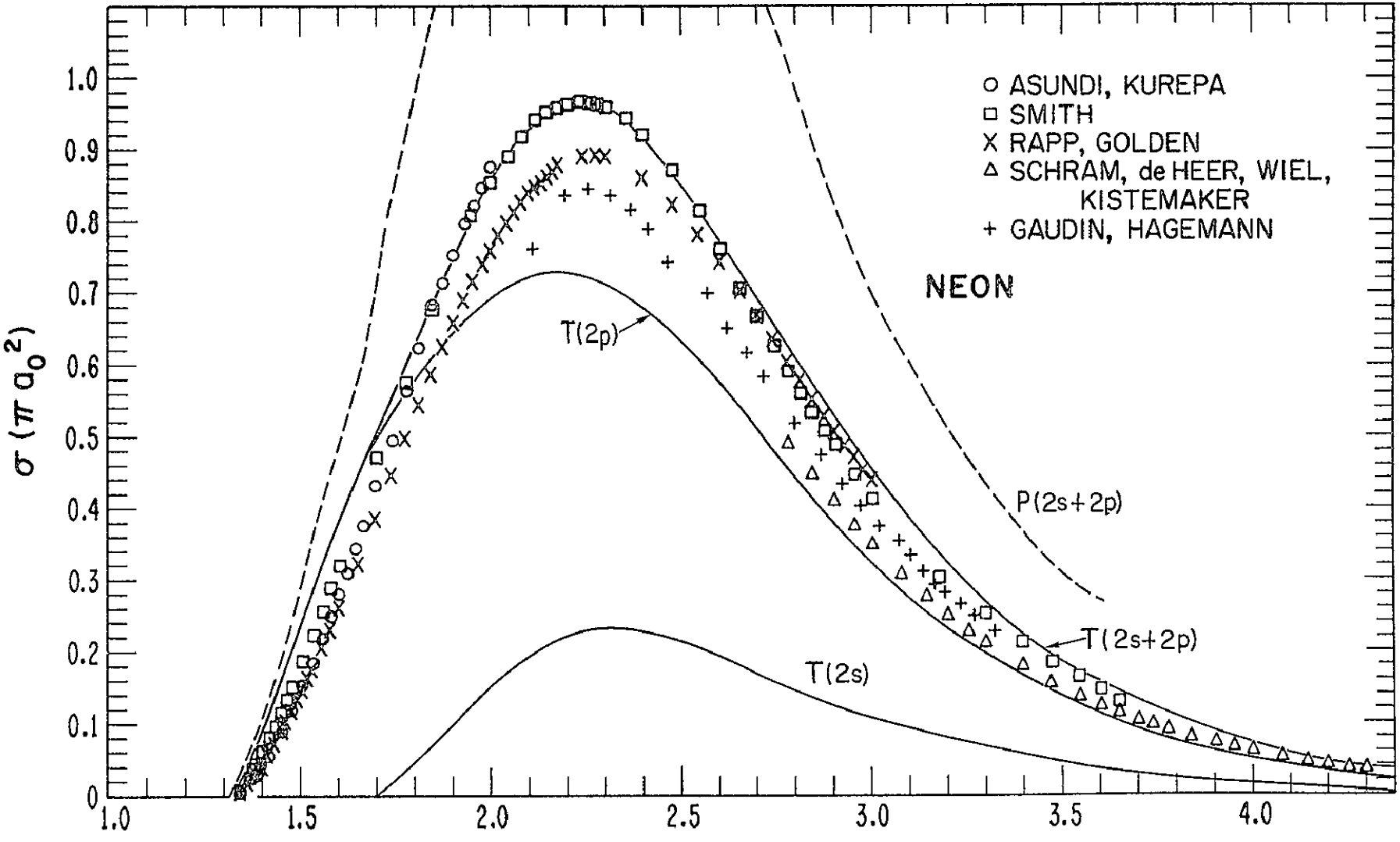
ASUNDI, KUREPA
SMITH
RAPP, GOLDEN
SCHRAM, de HEER, WIEL, KISTEMAKER
GAUDIN, HAGEMANN
NEON
T(2p)
P(2s+2p)
T(2s+2p)
T(2s)
σ (π a0²)
log10 E (eV)
1.0
0.9
0.8
0.7
0.6
0.5
0.4
0.3
0.2
0.1
0
1.0
1.5
2.0
2.5
3.0
3.5
4.0

FIG. 5

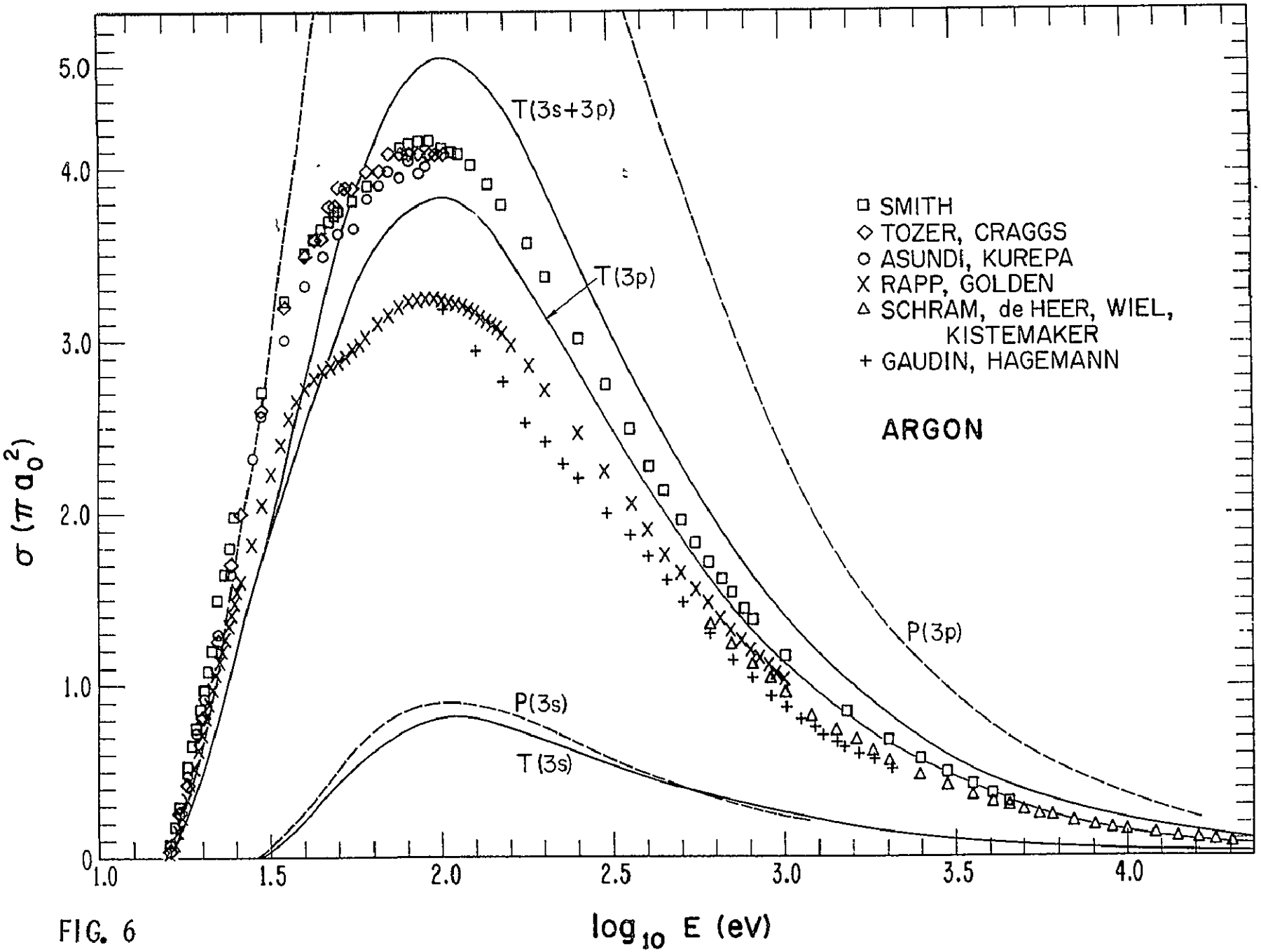
T(3s+3p)
T(3p)
P(3p)
P(3s)
T(3s)
SMITH
TOZER, CRAGGS
ASUNDI, KUREPA
RAPP, GOLDEN
SCHRAM, de HEER, WIEL, KISTEMAKER
GAUDIN, HAGEMANN
ARGON
σ (π a0²)
log10 E (eV)
0
1.0
2.0
3.0
4.0
5.0
1.0
1.5
2.0
2.5
3.0
3.5
4.0

FIG. 6

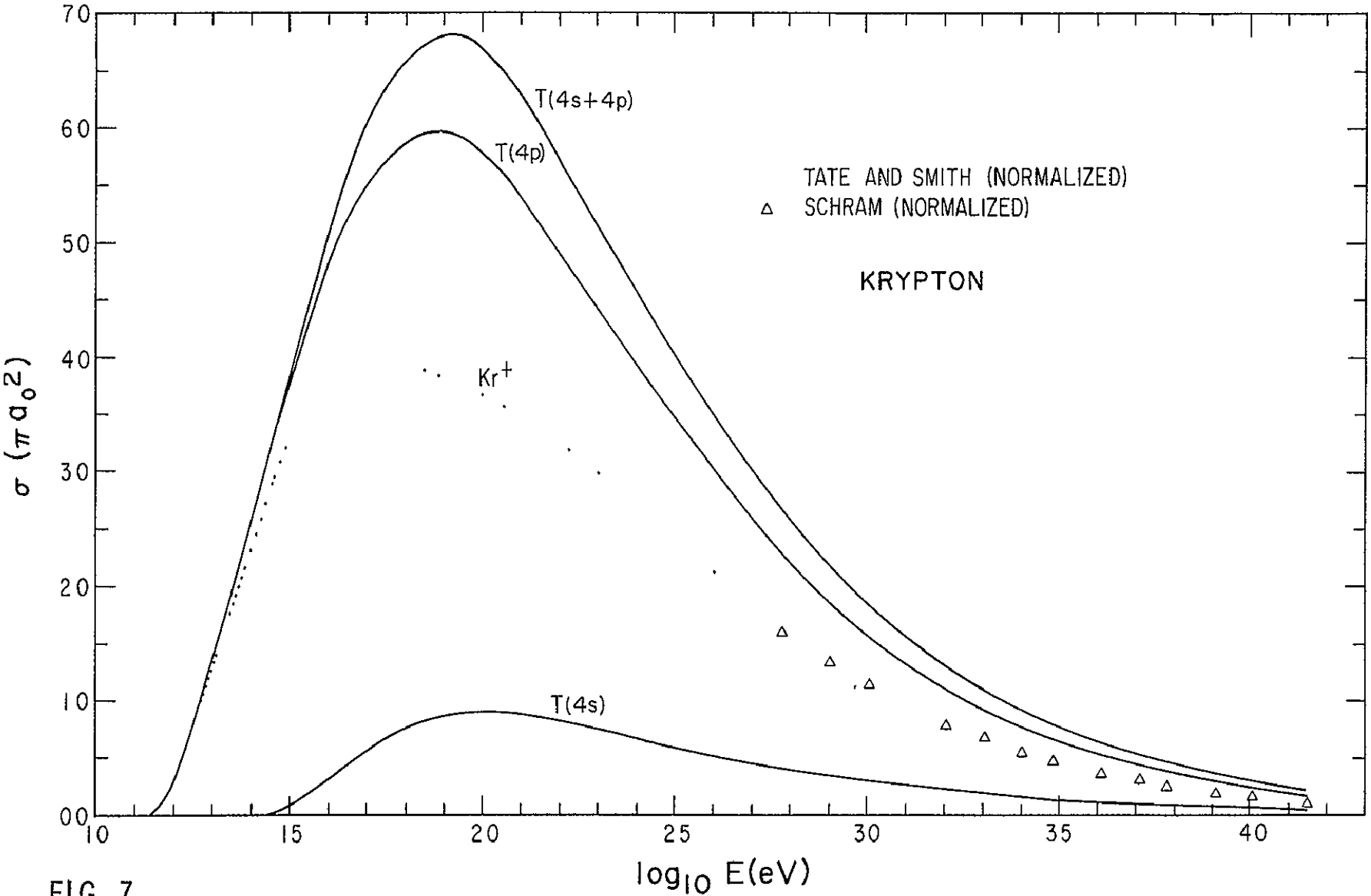
70
60
50
40
30
20
10
00
10
15
20
25
30
35
40
σ (πa₀²)
log₁₀ E(eV)
T(4s+4p)
T(4p)
T(4s)
Kr⁺
TATE AND SMITH (NORMALIZED)
SCHRAM (NORMALIZED)
KRYPTON

FIG. 7

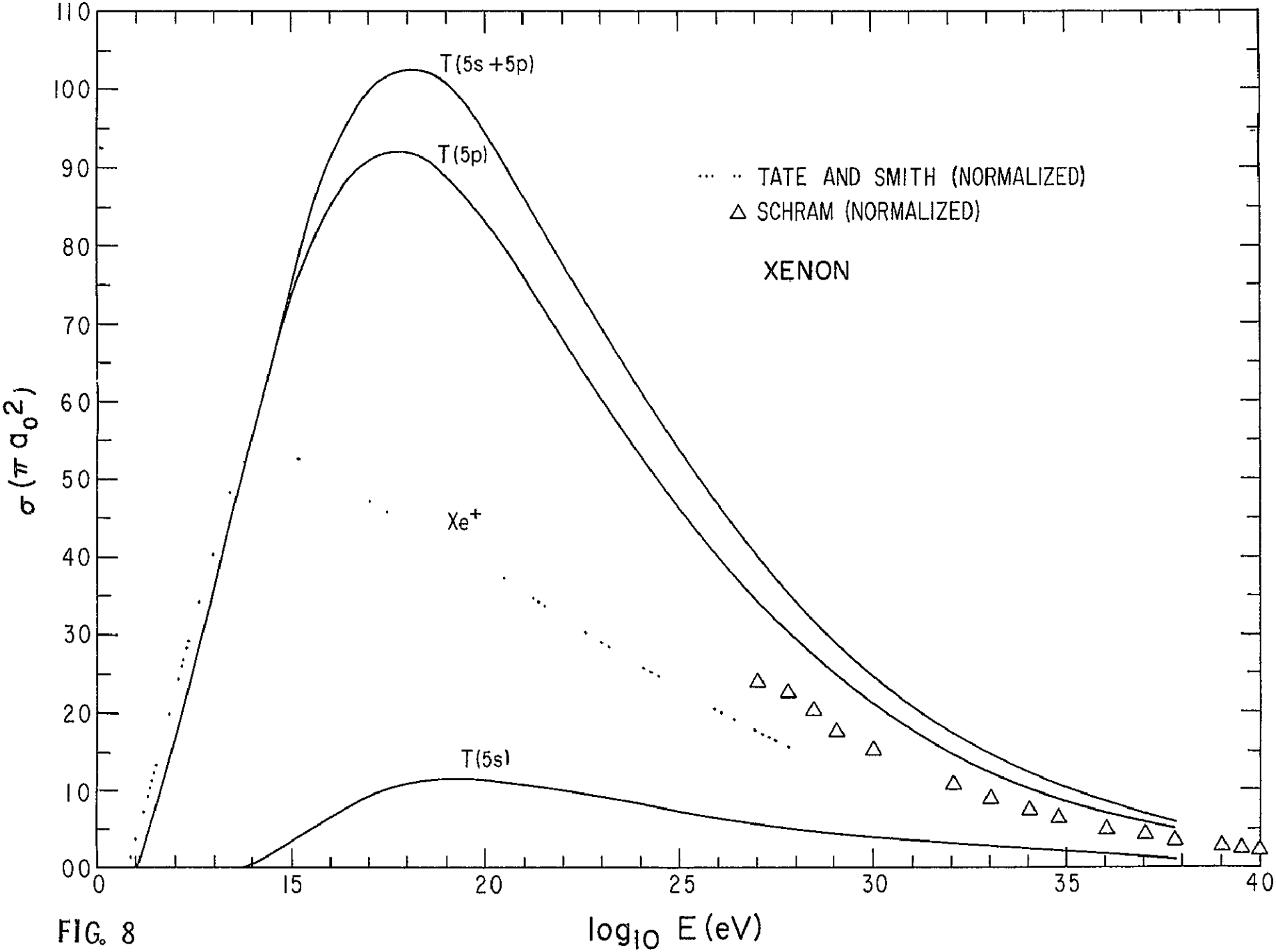
T(5s +5p)
T(5p)
TATE AND SMITH (NORMALIZED)
SCHRAM (NORMALIZED)
XENON
Xe+
T(5s)
σ (π a0 2)
log10 E (eV)
110
100
90
80
70
60
50
40
30
20
10
00
0
15
20
25
30
35
40

FIG. 8

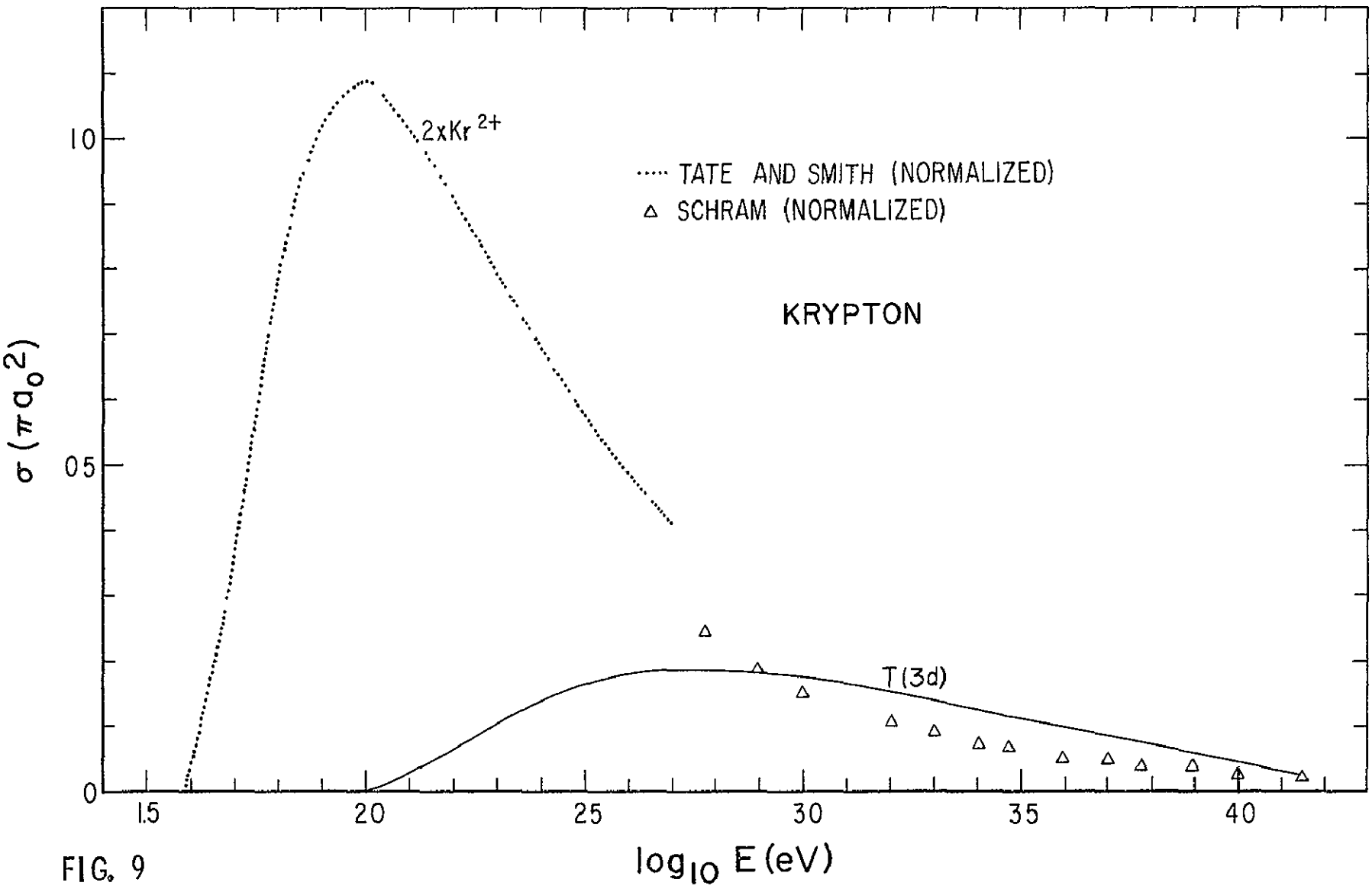
10
05
0
2xKr 2+
TATE AND SMITH (NORMALIZED)
SCHRAM (NORMALIZED)
KRYPTON
T(3d)
1.5
20
25
30
35
40
σ (πa0 2)
log10 E (eV)

FIG. 9

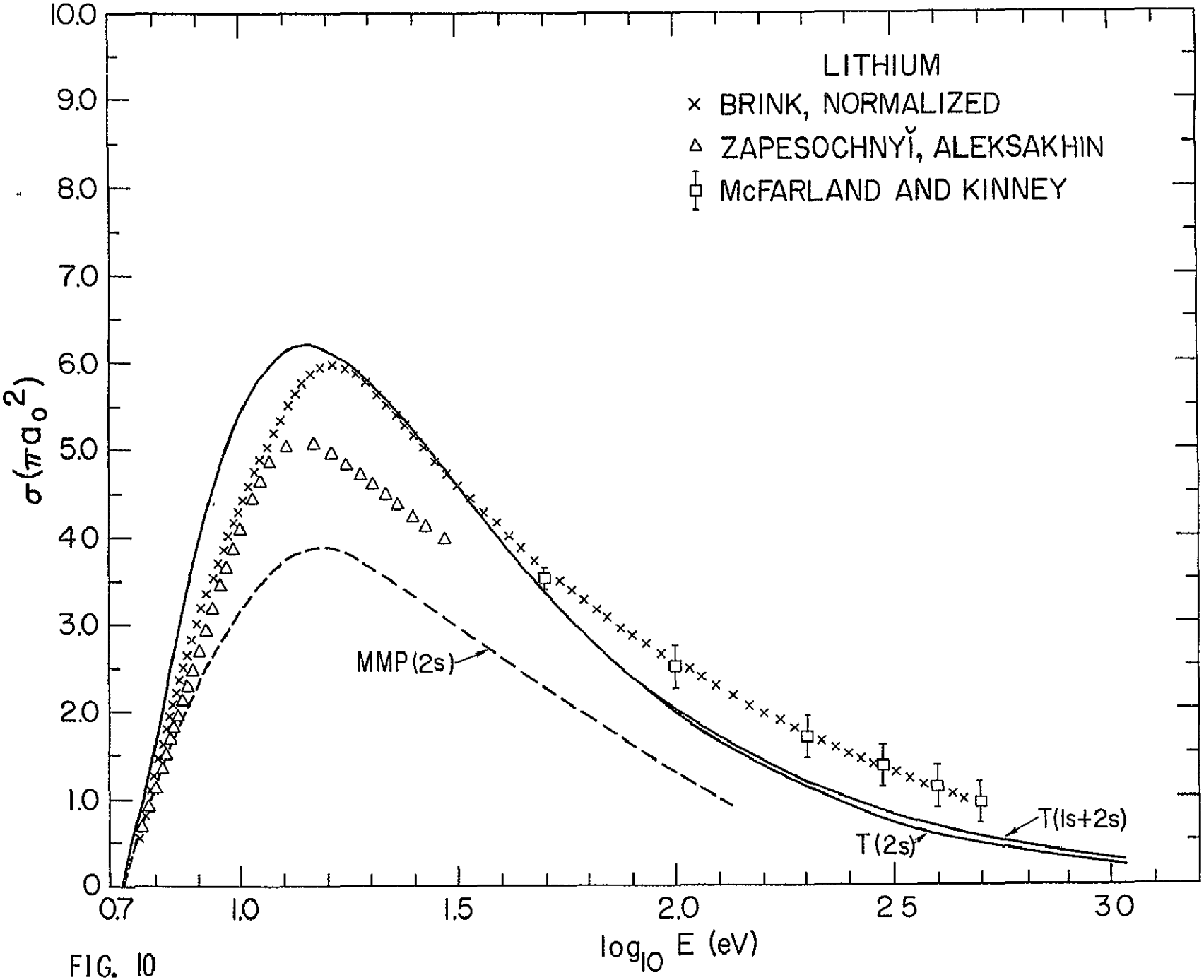
LITHIUM
× BRINK, NORMALIZED
△ ZAPESOCHNYĬ, ALEKSAKHIN
□ McFARLAND AND KINNEY
MMP(2s)
T(1s+2s)
T(2s)
σ(πa₀²)
log₁₀ E (eV)
10.0
9.0
8.0
7.0
6.0
5.0
4.0
3.0
2.0
1.0
0
0.7
1.0
1.5
2.0
2.5
3.0

FIG. 10

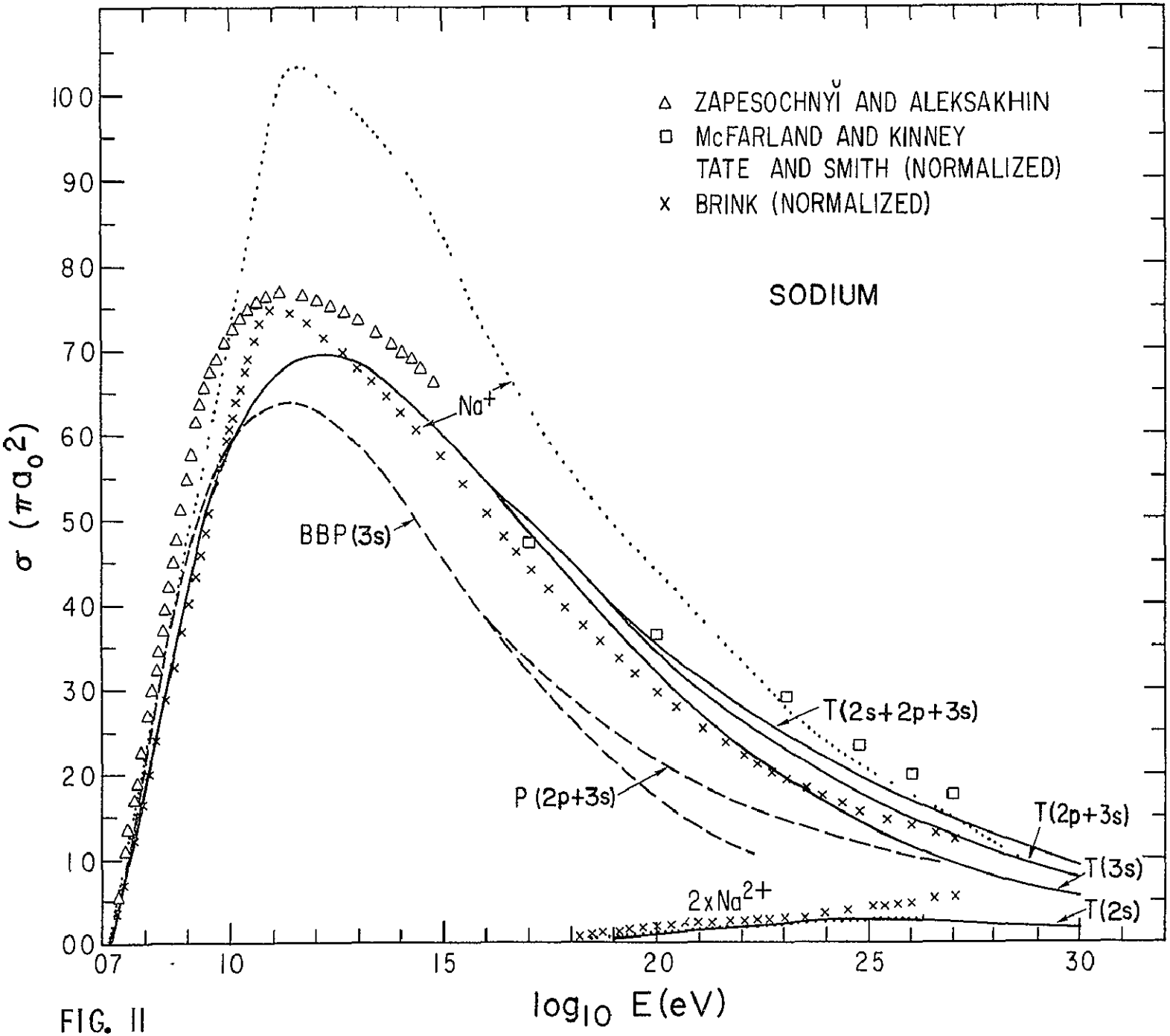
ZAPESOCHNYĬ AND ALEKSAKHIN
McFARLAND AND KINNEY
TATE AND SMITH (NORMALIZED)
BRINK (NORMALIZED)
SODIUM
Na+
BBP(3s)
P (2p+3s)
T(2s+2p+3s)
T(2p+3s)
T(3s)
T(2s)
2xNa2+
σ (πa0²)
log10 E(eV)
00
10
20
30
40
50
60
70
80
90
100
07
10
15
20
25
30

FIG. 11

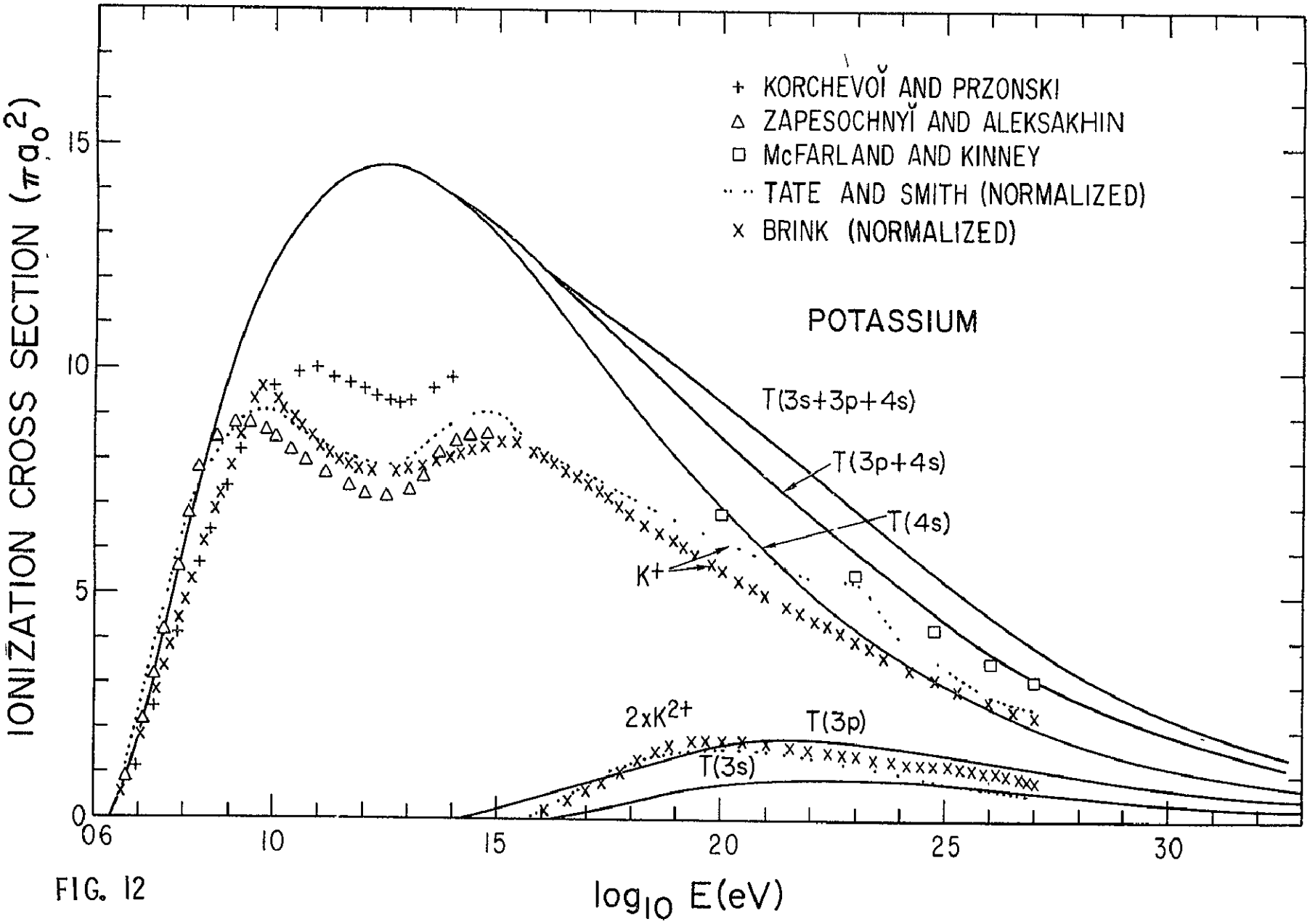
+ KORCHEVOĬ AND PRZONSKI
△ ZAPESOCHNYĬ AND ALEKSAKHIN
□ McFARLAND AND KINNEY
··· TATE AND SMITH (NORMALIZED)
× BRINK (NORMALIZED)
POTASSIUM
T(3s+3p+4s)
T(3p+4s)
T(4s)
K+
2xK2+
T(3p)
T(3s)
IONIZATION CROSS SECTION (πa0²)
log10 E(eV)
0
5
10
15
06
10
15
20
25
30

FIG. 12

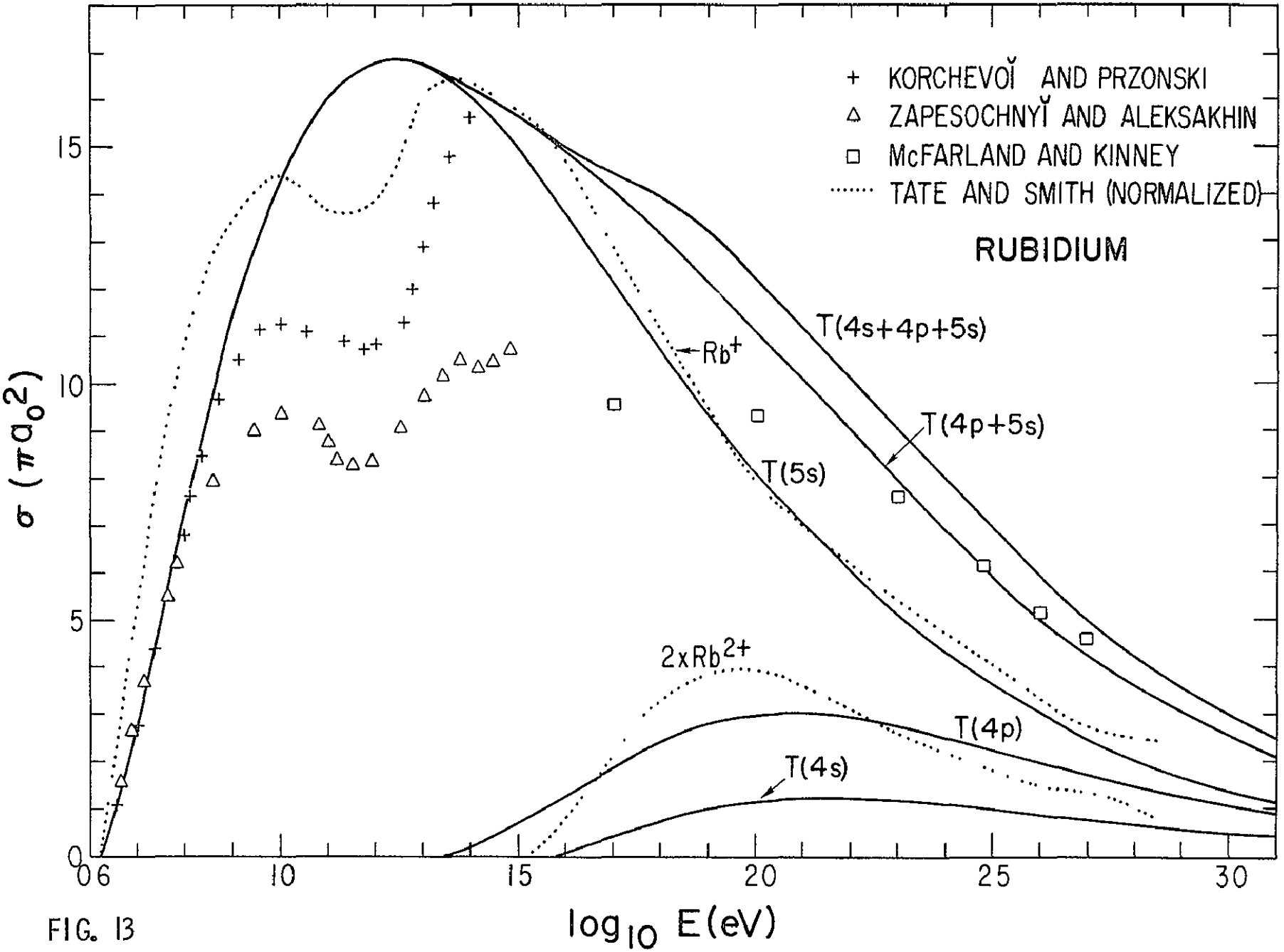
+ KORCHEVOĬ AND PRZONSKI
△ ZAPESOCHNYĬ AND ALEKSAKHIN
□ McFARLAND AND KINNEY
····· TATE AND SMITH (NORMALIZED)
RUBIDIUM
T(4s+4p+5s)
T(4p+5s)
T(5s)
Rb+
2xRb2+
T(4p)
T(4s)
σ (πa0^2)
log10 E(eV)
0
5
10
15
06
10
15
20
25
30

FIG. 13

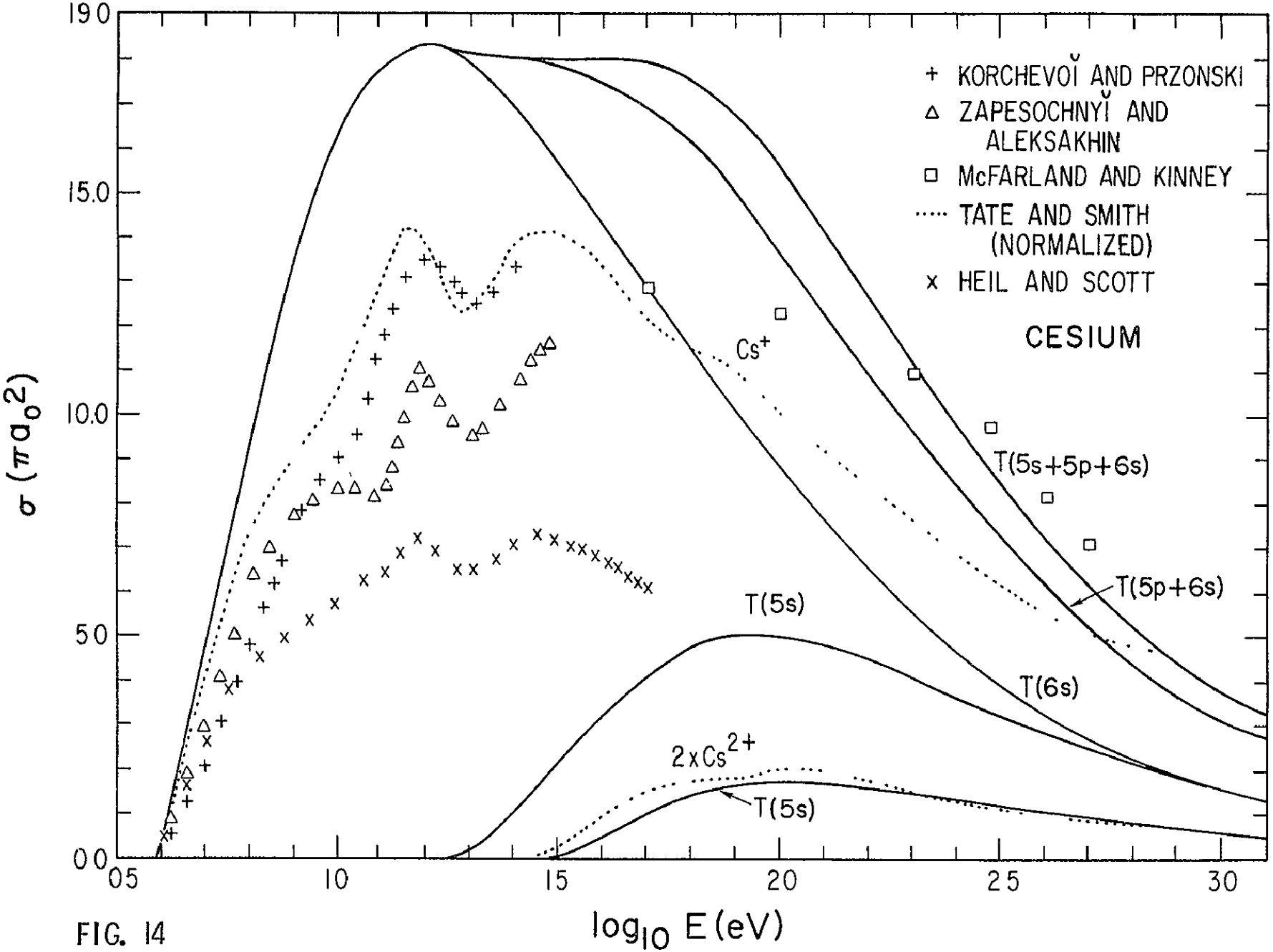
19.0
15.0
10.0
5.0
0.0
0.5
1.0
1.5
2.0
2.5
3.0
σ (πa₀²)
log₁₀ E (eV)
+ KORCHEVOĬ AND PRZONSKI
△ ZAPESOCHNYĬ AND ALEKSAKHIN
□ McFARLAND AND KINNEY
····· TATE AND SMITH (NORMALIZED)
× HEIL AND SCOTT
CESIUM
Cs+
T(5s+5p+6s)
T(5p+6s)
T(6s)
T(5s)
2xCs2+
T(5s)

FIG. 14

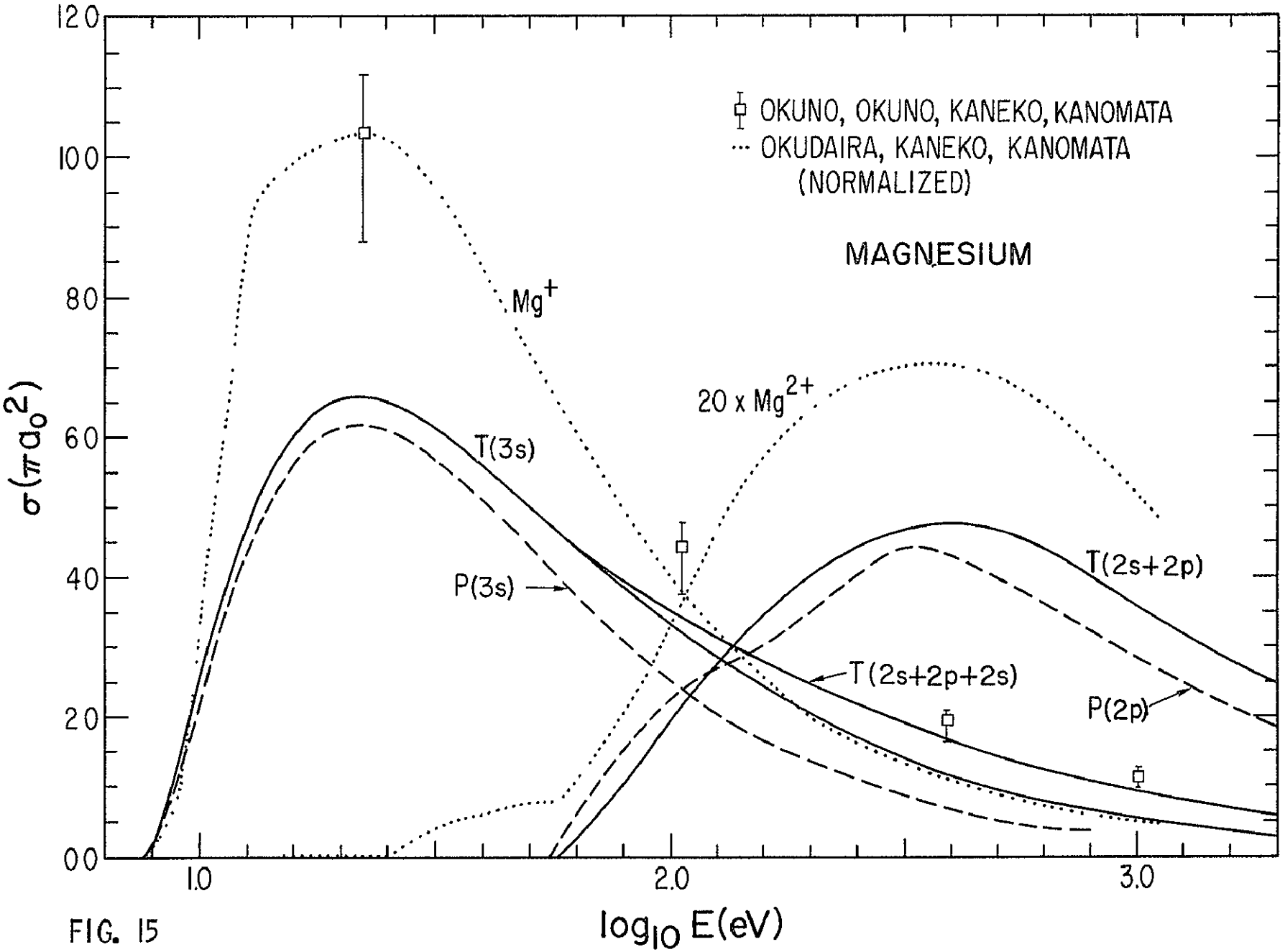
120
100
80
60
40
20
00
1.0
2.0
3.0
$\sigma(\pi a_0^2)$
$\log_{10} E(eV)$
OKUNO, OKUNO, KANEKO, KANOMATA
OKUDAIRA, KANEKO, KANOMATA
(NORMALIZED)
MAGNESIUM
Mg^+
$20 \times Mg^{2+}$
T(3s)
P(3s)
T(2s+2p)
T(2s+2p+2s)
P(2p)

FIG. 15

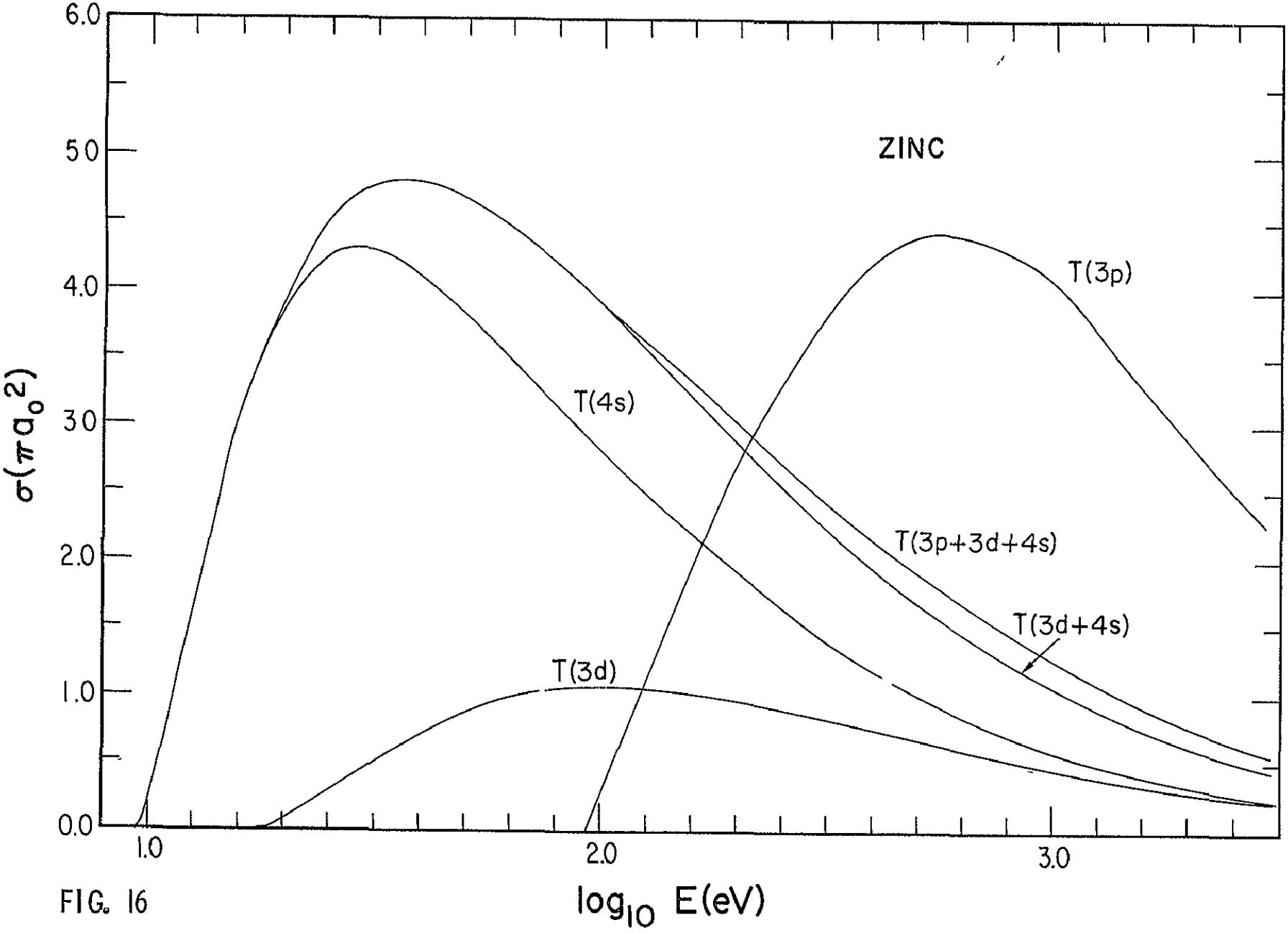
ZINC
T(3p)
T(4s)
T(3p+3d+4s)
T(3d+4s)
T(3d)
6.0
5.0
4.0
3.0
2.0
1.0
0.0
1.0
2.0
3.0
σ(πa₀²)
log₁₀ E(eV)

FIG. 16

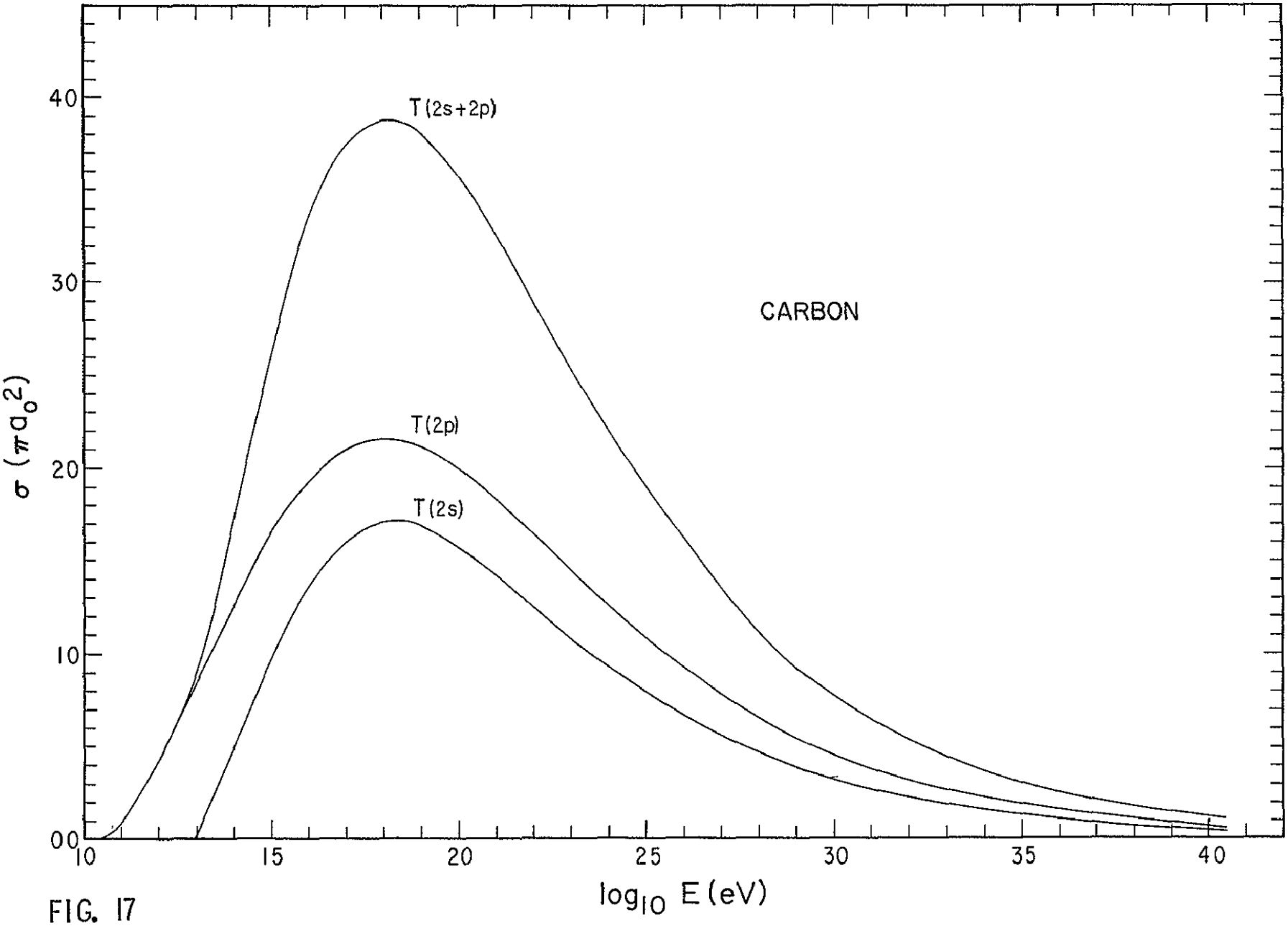
T(2s+2p)
T(2p)
T(2s)
CARBON
σ (πa₀²)
log₁₀ E (eV)
0
10
20
30
40
10
15
20
25
30
35
40

FIG. 17

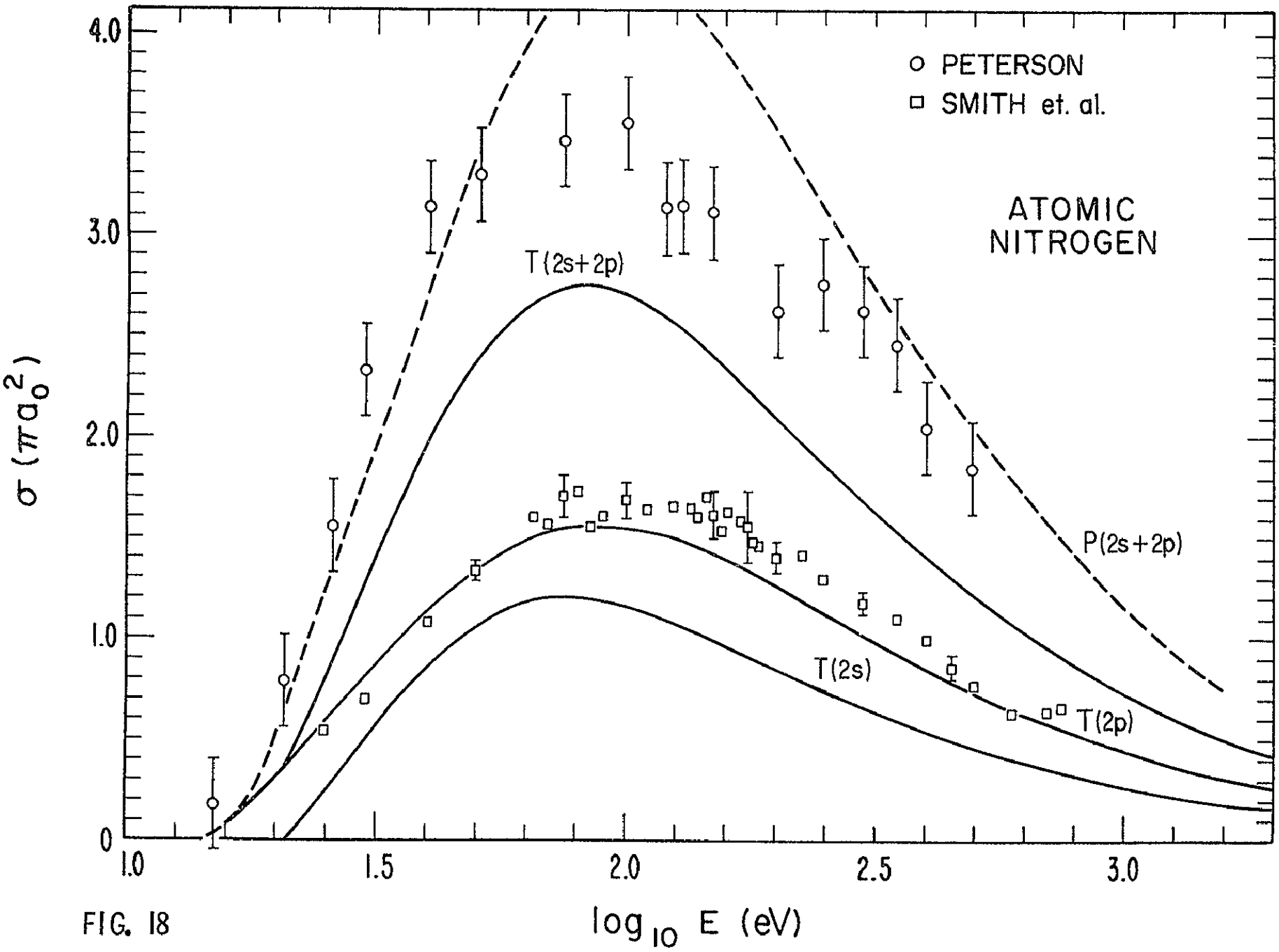
PETERSON
SMITH et. al.
ATOMIC
NITROGEN
T(2s+2p)
P(2s+2p)
T(2s)
T(2p)
σ (πa₀²)
log₁₀ E (eV)
4.0
3.0
2.0
1.0
0
1.0
1.5
2.0
2.5
3.0

FIG. 18

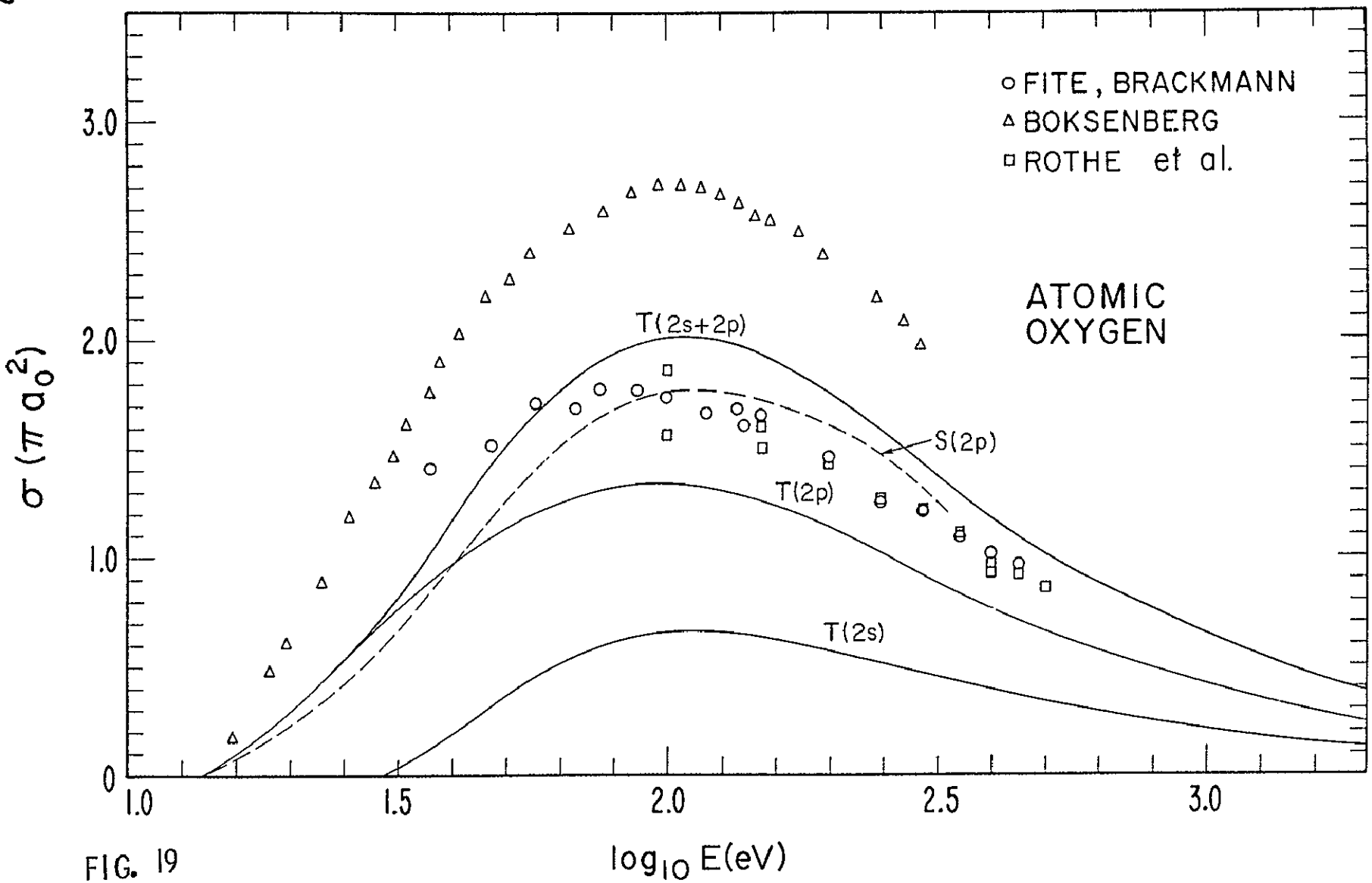
FITE, BRACKMANN
BOKSENBERG
ROTHE et al.
ATOMIC
OXYGEN
T(2s+2p)
S(2p)
T(2p)
T(2s)
σ (π a0²)
log10 E(eV)
0
1.0
2.0
3.0
1.0
1.5
2.0
2.5
3.0

FIG. 19

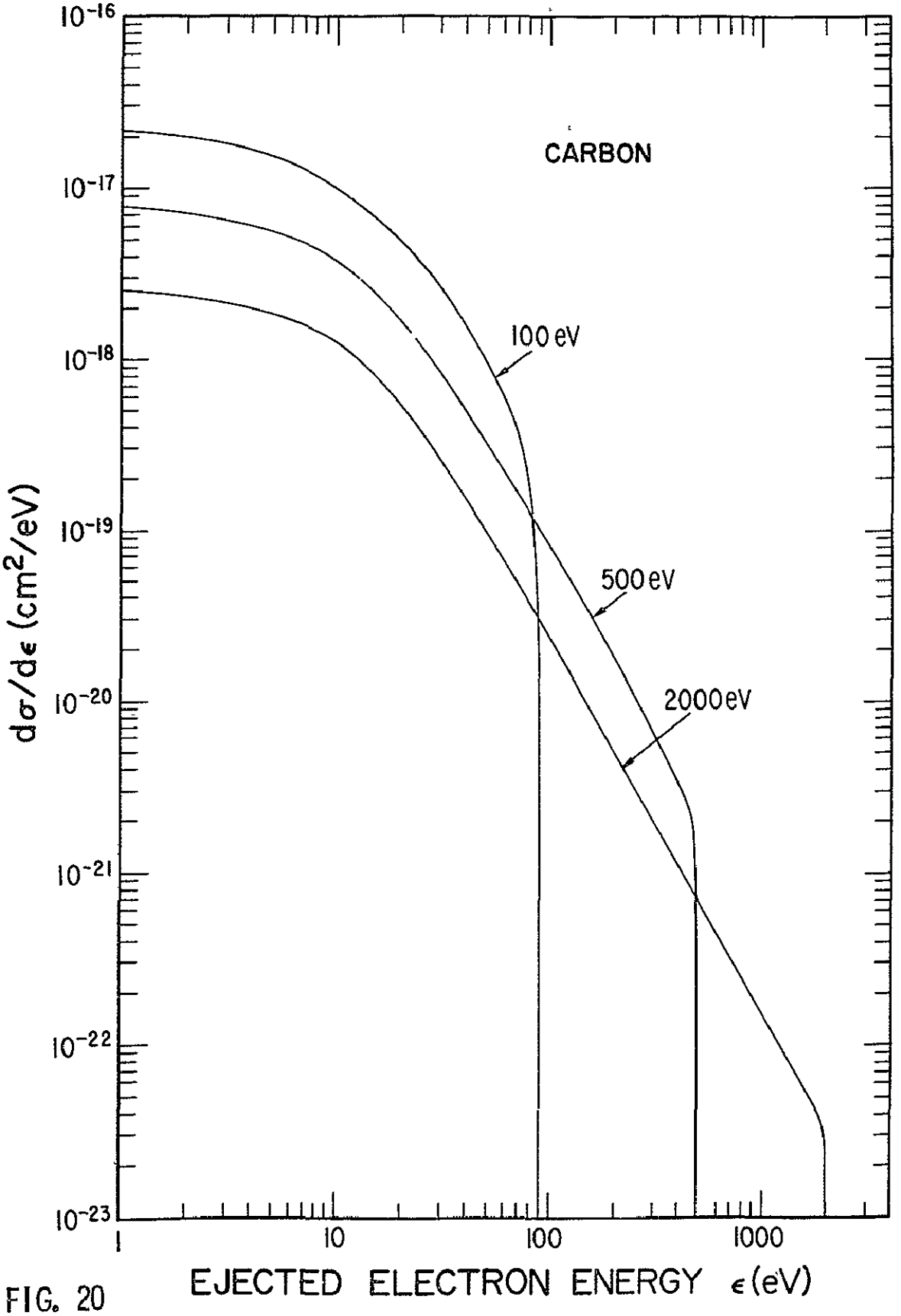
CARBON
100 eV
500 eV
2000 eV
10^{-16}
10^{-17}
10^{-18}
10^{-19}
10^{-20}
10^{-21}
10^{-22}
10^{-23}
$d\sigma/d\epsilon$ (cm^2/eV)
1
10
100
1000
EJECTED ELECTRON ENERGY ϵ (eV)

FIG. 20

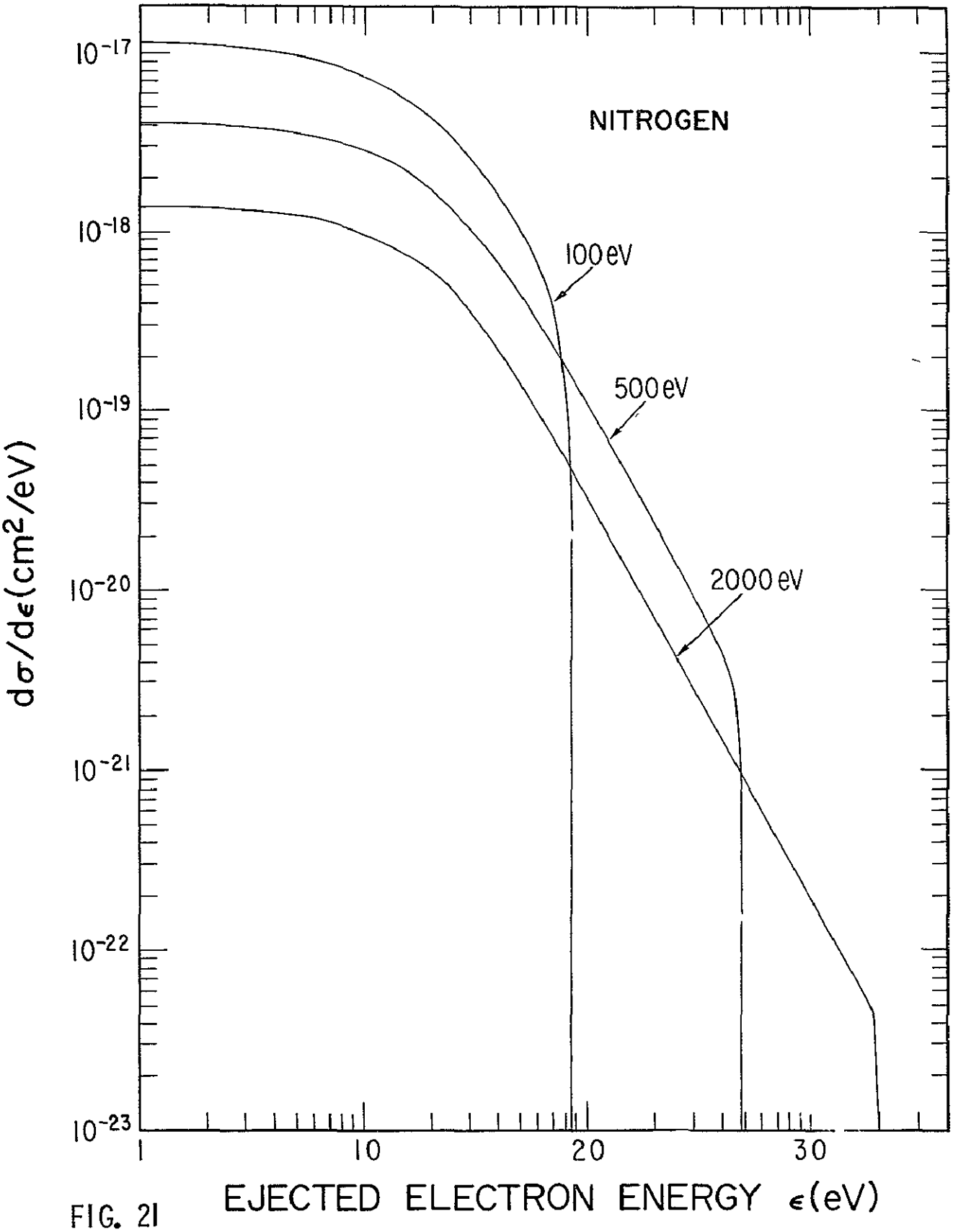
NITROGEN
100 eV
500 eV
2000 eV
10^{-17}
10^{-18}
10^{-19}
10^{-20}
10^{-21}
10^{-22}
10^{-23}
$d\sigma/d\epsilon(cm^2/eV)$
1
10
20
30
EJECTED ELECTRON ENERGY ϵ(eV)

FIG. 21

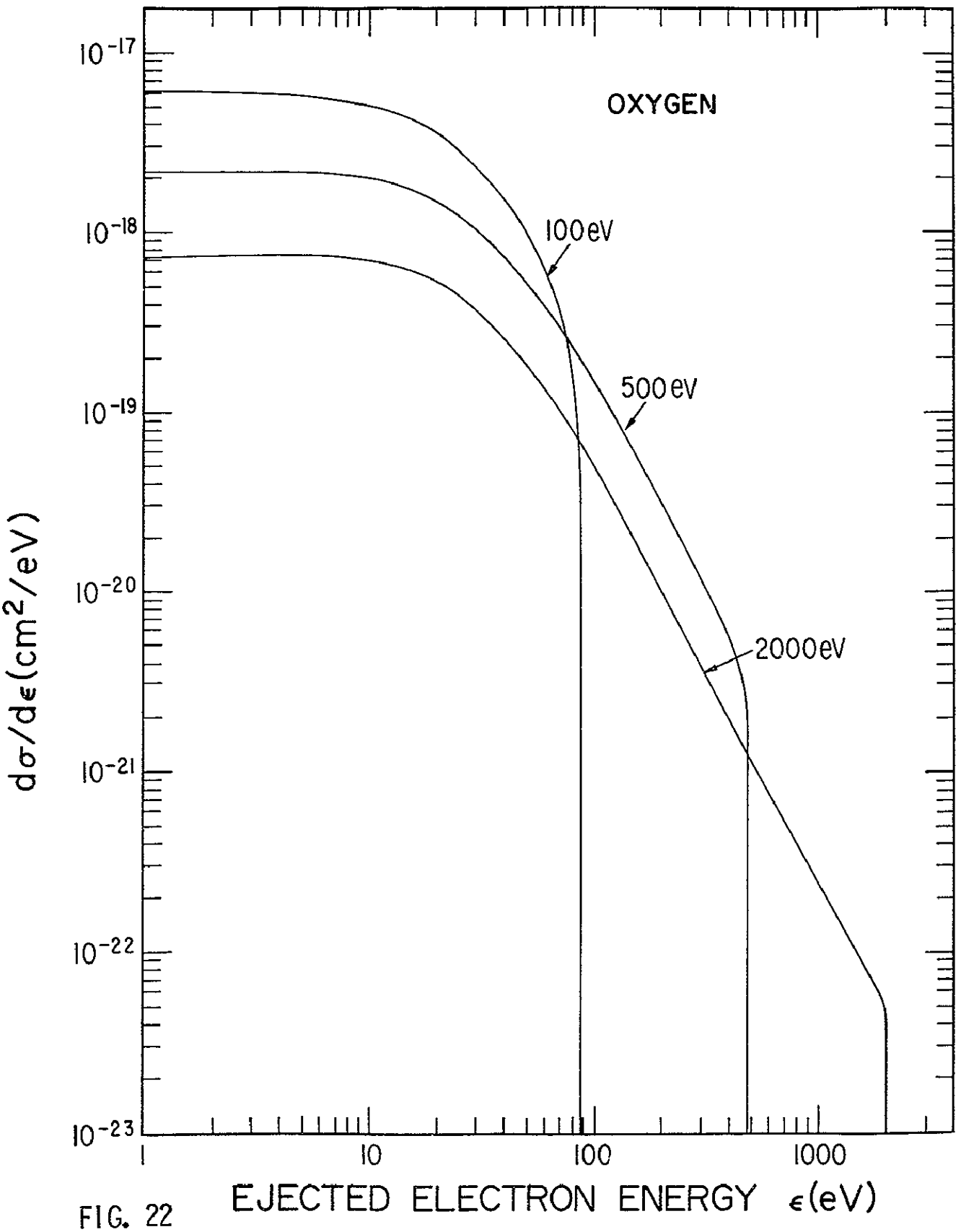
OXYGEN
100eV
500eV
2000eV
10^{-17}
10^{-18}
10^{-19}
10^{-20}
10^{-21}
10^{-22}
10^{-23}
$d\sigma/d\epsilon(cm^2/eV)$
10
100
1000
EJECTED ELECTRON ENERGY ϵ(eV)

FIG. 22

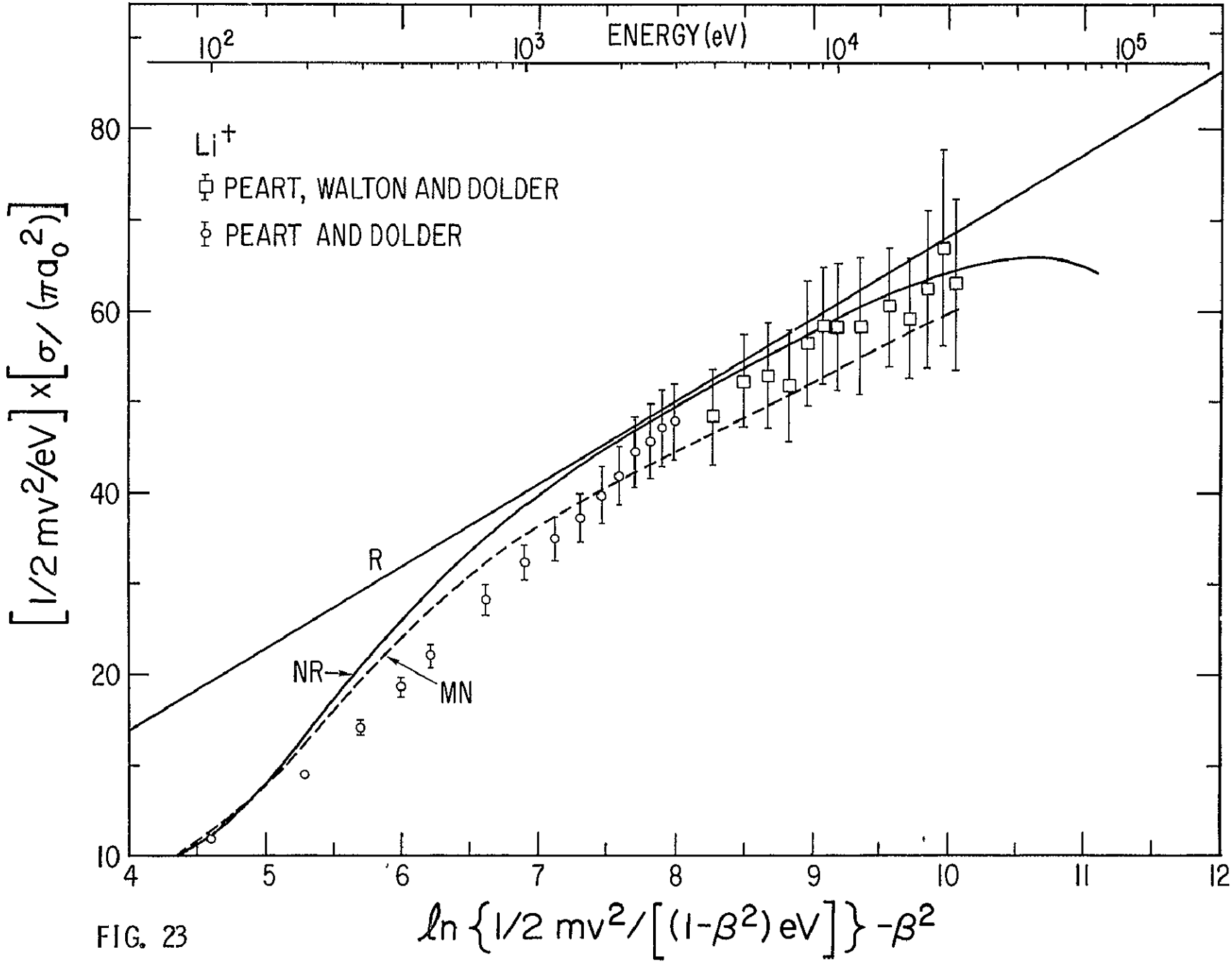
ENERGY (eV)
10^2
10^3
10^4
10^5
Li^+
PEART, WALTON AND DOLDER
PEART AND DOLDER
R
NR
MN
$[1/2\, mv^2/eV] \times [\sigma/(\pi a_o^2)]$
$\ln\{1/2\, mv^2/[(1-\beta^2)\, eV]\} - \beta^2$
10
20
40
60
80
4
5
6
7
8
9
10
11
12

FIG. 23